

Nonequilibrium thermodynamics of circulation regimes in optically-thin, dry atmospheres

Salvatore Pascale^a, Francesco Ragone^a, Valerio Lucarini^{a,b}, Yixiong Wang^c,
Robert Boschi^a

^a*KlimaCampus, Meteorologisches Institut, Universität Hamburg, Hamburg, Germany*

^b*Department of Mathematics and Statistics, University of Reading, Reading, U*

^c*Department of Physics, University of Oxford, Clarendon Laboratory, Parks Road,
Oxford, UK*

Abstract

An extensive analysis of an optically-thin, dry atmosphere at different values of the thermal Rossby number \mathcal{Ro} and of the Taylor number \mathcal{F}_f is performed with a general circulation model by varying the rotation rate Ω and the surface drag τ in a wide parametric range. By using nonequilibrium thermodynamics diagnostics such as material entropy production, efficiency, meridional heat transport and kinetic energy dissipation we characterize in a new way the different circulation regimes. Baroclinic circulations feature high mechanical dissipation, meridional heat transport, material entropy production and are fairly efficient in converting heat into mechanical work. The thermal dissipation associated with the sensible heat flux is found to depend mainly on the surface properties, almost independent from the rotation rate and very low for quasi-barotropic circulations and regimes approaching equatorial super-rotation. Slowly rotating, axisymmetric circulations have the highest meridional heat transport. At high rotation rates and intermediate-high drag, atmospheric circulations are zonostrophic with very low mechanical dissipation, meridional heat transport and efficiency. When τ is interpreted as a tunable parameter associated with the turbulent boundary layer transfer of momentum and sensible heat, our results confirm the possibility of using the Maximum Entropy Production Principle as a tuning guideline in the range of values of Ω . This study suggests the effectiveness of using fundamental nonequilibrium thermodynamics for investigating the properties of planetary atmospheres and extends our knowledge of the thermodynamics of the atmospheric circulation regimes.

Keywords: Circulation regimes, nonequilibrium thermodynamics, terrestrial planetary atmospheres, baroclinic instability, entropy production
2010 MSC: 85A20, 80A17, 86A10, 76U05, 37G35

1. Introduction

In the last two decades, more than 700 planets outside the solar system (exoplanets) have been discovered (Udry and Santos, 2007), and the Kepler Space Telescope has recently located over 2,000 exoplanet candidates (Borucki et al., 2011). The study of exoplanets and their climates is in its early stage and it is quickly developing (Seager and Deming, 2010). Observational data are still poor and difficult to obtain, particularly for those planets – super-Earths (Charbonneau et al., 2009) – that might be capable of sustaining liquid water and thus potentially suitable for life. Nevertheless, the discovery of exoplanets is extending the scope of planetary sciences towards the study of the so-called “exoclimates” (Heng, 2012; Burrows et al., 1997; Heng et al., 2011a; Showman et al., 2009; Joshi, 2003; Merlis and Schneider, 2010; Lewis et al., 2010; Pierrehumbert, 2010; Thrastarson and Cho, 2011; Rauscher and Menou, 2012; Dobbs-Dixon et al., 2012). Exoplanets and their atmospheres are in general capable of supporting a broad set of circulation regimes since they are characterized by a range of physical (atmospheric composition, rotation rate, dimension, surface) and orbital (obliquity, eccentricity, distance from the parental star, spectral type of the parental star, presence or not of phase locking) parameters even wider than that of Solar System planets (Williams and Pollard, 2002). Planetary science aims at predicting and classifying in a concise but comprehensive way exoclimates once the main orbital and physical parameters are known.

Recently Read (2011) noted that the large variety of circulation regimes may be better understood by adopting the fluid-dynamical method of similarity, i.e. by defining a set of dimensionless numbers that fully characterise the planetary circulations. Two climate states that share the same set of dimensionless numbers are dynamically equivalent and so the statistical properties of one can be mapped onto those of the other. Obviously the set of parameters is fairly large, and one of the main objectives of planetary science is to understand what is the minimal number of dimensionless parameters needed to define virtually equivalent circulations (Wang, 2012; Showman et al., 2010). In this study we focus on the impact of two parameters, the rotation rate Ω

33 and on the surface turbulent exchange rate τ , on the atmospheric circulation
34 of an Earth-like dry atmosphere. The choice of such parameters naturally
35 leads to the definition of two dimensionless numbers, the thermal Rossby
36 number $\mathcal{R}o$ and the Taylor (frictional) number \mathcal{F}_f (Read, 2011).

37 Over the last three decades, the effect of the planetary rotation on at-
38 mospheric circulation has been investigated in some details with the aid of
39 general circulation models (Hunt, 1979; Williams, 1988a,b; Navarra and Boc-
40 caletti, 2002; Genio and Suozzo, 1987; Geisler et al., 1983; Read, 2011; Vallis
41 and Farneti, 2009). Variations in the value of Ω impacts directly the size of
42 the baroclinic waves and the extent of the Hadley cell, which are the main
43 features of the large-scale Earth atmospheric circulation. The size of the
44 baroclinic disturbances, being proportional to the Rossby deformation ra-
45 dius (Eady, 1949), scales as $1/\Omega$. The latitudinal extent of the Hadley cell
46 also scales as $1/\Omega$ (Held and Hou, 1980). Numerical simulations of slowly
47 rotating Earth-like planets and of Solar System planets like Venus and Ti-
48 tan (Clancy et al., 2007; Hourdin et al., 1995) have shown the presence of
49 one poleward-extended Hadley cell in each hemisphere and the weakening
50 or complete disappearing of the midlatitude baroclinic disturbances. On the
51 other hand, at fast rotation rates the emergence of multiple cells in the merid-
52 ional circulation and multiple jets in the zonal circulation has been observed
53 both in numerical simulations (Williams, 1988a, 1978) and observations (e.g.
54 Jupiter).

55 The dynamical effects of the solid lower boundary of terrestrial planets
56 on the atmospheric circulation is also quite important in order to understand
57 planetary circulations and has not been fully addressed yet (Showman et al.,
58 2010). The characteristics of the surface have been recognised as a key factor
59 in shaping Earth’s atmospheric circulation (James, 1994; James and Gray,
60 1986), although this topic has received less attention than that related to Ω .
61 The surface of a terrestrial planet, due to its roughness, affects the turbulent
62 flow within the planetary boundary and thus the exchange of momentum and
63 energy between the surface and the atmosphere (Arya, 1988). It has been
64 shown (James and Gray, 1986; James, 1987; Kleidon et al., 2003) that the
65 reduction of the surface drag leads to strong horizontal barotropic shears in
66 the zonal mean flow. By using a two-level quasi-geostrophic model, James
67 (1987) showed that the growth rate of the most unstable baroclinic modes is
68 reduced considerably by the strong horizontal wind shears. This is related to
69 the general fact that the linearised baroclinic instability equations obey the
70 Squire’s theorem (Kundu and Cohen, 2004). The role of drag has received

71 some attention in the exoplanets context (Rauscher and Menou, 2012) but,
72 to the authors' knowledge, has not been systematically investigated so far
73 for rotation rates which are different from the Earth's. In this study we
74 investigate the combined effect of rotation speed and surface roughness on
75 the dynamics, linking it to the nonequilibrium thermodynamics of the system.

76 Thermodynamics provide a way for characterizing concisely a complex
77 physical system, bringing together comprehensive but minimal physical in-
78 formation. The atmosphere of a planet is an example of a nonequilibrium
79 system (Gallavotti, 2006; DeGroot and Mazur, 1984; Kleidon, 2009), and its
80 general circulation redistributes energy in order to compensate for the ra-
81 diative differential heating between hot and cold regions. The atmospheric
82 circulation therefore is fuelled by the conversion of available potential energy
83 due to large temperature gradients into kinetic energy. The atmosphere, in
84 other terms, produces mechanical work, acting as a heat engine (Lorenz,
85 1967; Peixoto et al., 1991; Johnson, 2000; Lucarini, 2009). It seems therefore
86 natural to adopt nonequilibrium thermodynamics as a general framework for
87 studying exoclimates. Such an approach has been, for example, applied in
88 Lucarini et al. (2010) and Boschi et al. (2012) for studying the bistability of
89 an Earth-like planet. Furthermore, thermodynamical disequilibrium drives
90 a variety of irreversible processes, from frictional dissipation to chemical re-
91 actions. The irreversibility of climatic processes is quantified by the mate-
92 rial entropy production (Goody, 2000; Kleidon and Lorenz, 2005; Kleidon,
93 2009). The interest in studying climate material entropy production largely
94 stemmed from the proposal of the maximum entropy production principle
95 (MEPP) by Paltridge (Paltridge, 1975, 1978, 2001), who suggested that the
96 climate adjusts in such a way as to maximize the material entropy produc-
97 tion. In its weak form, the MEPP suggests to use the entropy production
98 as a target function to be maximized when tuning an empirical or uncertain
99 parameter of a model (Kleidon et al., 2003; Kunz et al., 2008). Whereas the
100 theoretical foundations of MEPP are still unclear (Dewar, 2005; Grinstead
101 and Linsker, 2007; Goody, 2007), such a conjecture has also been proposed
102 as a way to estimate the meridional heat transport of other planets, such
103 as Mars and Titan (Lorenz et al., 2001; Jupp and Cox, 2010) and poten-
104 tially to exoplanets too, and has stimulated the re-examination of climatic
105 dissipative processes (Peixoto et al., 1991; Goody, 2000; Pauluis and Held,
106 2002a,b; Kleidon and Lorenz, 2005; Fraedrich and Lunkeit, 2008; Pascale
107 et al., 2011a).

108 In this study we perform a large ensemble of numerical simulations with

109 an Earth-like general circulation model for many different values of Ω and τ in
 110 order to compute the dissipative properties ζ (where ζ is any dissipative func-
 111 tion, e.g. material entropy production) of circulations of dry atmospheres at
 112 different thermal Rossby and Taylor numbers, $\zeta(\mathcal{R}o, \mathcal{F}_f)$. We relate, for the
 113 first time, the properties of $\zeta(\mathcal{R}o, \mathcal{F}_f)$ to the different circulation regimes and
 114 extend our knowledge on the global thermodynamic properties of rotating
 115 fluids. We anticipate that particular regimes (e.g. baroclinic, zonostrophic,
 116 super-rotation) are effectively characterized in terms of their thermodynamic
 117 properties. We conclude with a brief analysis of how effectively the MEPP
 118 can be used to infer the optimal value for an uncertain or empirical parame-
 119 ter, in this case exactly the time scale controlling the exchange of momentum
 120 and energy between free atmosphere and the surface.

121 The paper is organized as follows, In Section 2 we will shortly discuss
 122 the dimensionless parameters relevant for this study. In Section 3 the model
 123 and the experimental setup are presented. The characterization of different
 124 dynamical regimes is the subject of Section 4 whereas in Section 5 the ther-
 125 modynamical properties of the circulation regimes are analysed. In Section
 126 6 the main conclusions are summarized.

127 **2. Parametric range of general circulations and dimensionless num-** 128 **bers**

129 The role of the rotation rate in planetary circulations has been first inves-
 130 tigated in laboratory experiments with a thermally driven rotating annulus
 131 (Hide, 1953, 1969; Hide and Mason, 1975; Read et al., 1998; Read, 2001;
 132 Wordsworth et al., 2008; Hide, 2010). The system consists of a fluid confined
 133 between coaxial cylinders maintained at two different temperatures and ro-
 134 tating at an angular velocity Ω . When the basic parameters Ω and ΔT
 135 (temperature difference between the inner and outer cylinder) are varied, a
 136 wide variety of flow patterns is observed. Different dynamical regimes can be
 137 identified if results are grouped with respect to two dimensionless parameters,
 138 the *thermal Rossby number*:

$$\mathcal{R}o = \frac{g\alpha D\Delta T}{\Omega^2 L^2}, \quad (1)$$

139 and the *Taylor number*:

$$\mathcal{T}a = \frac{4\Omega^2 L^5}{\nu^2 D}, \quad (2)$$

140 in which L is the channel width, D its depth, ν the kinematic viscosity
 141 of the fluid, α its volumetric expansion coefficient, and g the gravitational
 142 acceleration.

143 Read (2011) has extended the definition of the thermal Rossby number
 144 and of the Taylor number to the case of atmospheric circulations. The anal-
 145 ogous of the thermal Rossby number is defined as:

$$\mathcal{R}_O = \frac{R\Delta\theta_h}{\Omega^2 a^2}, \quad (3)$$

146 where a is the planet’s radius, R the specific gas constant and $\Delta\theta_h$ the hor-
 147 izontal (potential) temperature contrast between equator and poles. A dif-
 148 ference between the definitions in eq. (1) and eq. (3) is that $\Delta\theta_h$ is not
 149 fixed externally but rather determined by the circulation itself. In the fol-
 150 lowing we will take $\Delta\theta_h = \Delta\theta_{hE}$, as done for example in Mitchell and Vallis
 151 (2010), where θ_{hE} is the radiative-convective equilibrium potential temper-
 152 ature, since this is externally determined by the incoming stellar radiative
 153 energy and thus a more objective quantity to describe the horizontal differ-
 154 ential driver for the circulation. A Taylor number can be defined analogously
 155 to the case of the rotating annulus as:

$$\mathcal{F}_f = 4\Omega^2\tau_f^2 \quad (4)$$

156 in which τ_f is the typical timescale for kinetic energy dissipation. We note
 157 that $\mathcal{F}_f \propto (\tau_f/\tau_{rot})^2$, where $\tau_{rot} = 2\pi/\Omega$, i.e. \mathcal{F}_f is proportional to the
 158 ratio of (the squares of) the typical timescales associated with turbulent
 159 dissipation of kinetic energy and rotation. For planets with a solid core, τ_f is
 160 the surface drag timescale and is in general determined by the characteristics
 161 of the surface. The use of (3) and (4) has been proved to be very useful in
 162 classifying atmospheric circulation (Wang, 2012).

163 3. Model and experimental setup

164 3.1. The Planet Simulator

165 Numerical simulations have been performed with the Planet Simulator
 166 (PlaSim), a general circulation model of intermediate complexity (Fraedrich
 167 et al., 2005). The model is freely available at www.mi.uni-hamburg.de/plasim.
 168 PlaSim is a fast running model and it is therefore suitable for large-ensemble
 169 numerical experiments. Moreover, a full set of thermodynamic diagnostics

170 is available, thus making it well suited for this work (Fraedrich and Lunkeit,
171 2008; Lucarini et al., 2010).

172 The atmospheric dynamic core uses the primitive equations, which are
173 solved using a spectral transform method (Eliassen et al., 1970; Orszag, 1970).
174 Interaction between radiation and atmosphere is dealt with using simple but
175 realistic longwave (Sasamori, 1968) and shortwave (Lacis and Hansen, 1974)
176 radiative schemes. In particular the incoming solar flux F_{SW}^{toa} at the top of
177 the atmosphere (TOA) is

$$F_{SW}^{toa} = S_0 \cos Z \quad (5)$$

178 where S_0 is the solar constant (1365 W m^{-2}) and Z the zenith angle, which
179 is in general a function on the latitude, time of the year and time of the
180 day, and it is computed following Berger (1978). All simulations have been
181 performed with orbital parameter – obliquity, eccentricity, distance from the
182 Sun, typical of Earth. Other sub-grid scale parametrisations include interac-
183 tive clouds (Stephens, 1978; Stephens et al., 1982; Slingo and Slingo, 1991),
184 moist (Kuo, 1965, 1974) and dry convection, large scale precipitation, bound-
185 ary layer fluxes and vertical and horizontal diffusion (Louis, 1979; Louis et al.,
186 1981; Laursen and Eliassen, 1989). More information can be found in PlaSim
187 reference manual, freely available at www.mi.uni-hamburg.de/Downloads-un.245.0.html.
188

189 In all simulations the lower boundary is a flat surface with prescribed
190 albedo and heat capacity (see Table 1). This is implemented with a shallow
191 energy-conserving slab-ocean model with an areal heat capacity ($C_{slab} = 10^7$
192 $\text{JK}^{-1} \text{m}^{-2}$) comparable to that chosen in Frierson et al. (2006) and Heng et al.
193 (2011b). In this way we avoid fixed surface temperature and have a simple
194 but energetically consistent climate model. The surface temperature evolves
195 in time according to $C_{slab} \dot{T}_s = F_{SW}^{surf} + F_{LW}^- = \sigma T_s^4 - F_T$ (F_{SW}^{surf} net solar
196 radiation at the surface, F_{LW}^- downward longwave radiation at the surface,
197 F_T surface sensible heat flux). We set the depth of the mixed layer to 5 m
198 in order to have an areal heat capacity ($C_{slab} = 10^7 \text{ JK}^{-1} \text{m}^{-2}$) comparable
199 to that chosen in Frierson et al. (2006) and Heng et al. (2011b). We have
200 checked our result at $C_{slab} = 10^8 \text{ JK}^{-1} \text{m}^{-2}$ too, finding little effects on the
201 circulations and on the global thermodynamical properties. Simulations are
202 performed at T42 spectral resolution ($2.8^\circ \times 2.8^\circ$) with ten levels (T42/10LEV
203 in the following).

204 In this study we consider dry atmospheres. Dry atmospheres are relevant
205 for planetary (e.g. Mars) and paleoclimatological (e.g. Snowball Earth) stud-

206 ies and, moreover, allow us to avoid the role of phase transitions associated
 207 with condensing substances, simplifying the problem and making neater the
 208 connection between dynamics and thermodynamics of the system. Such con-
 209 figuration is obtained by switching off the surface evaporation module and
 210 starting from a dry atmospheric condition. Water vapour is consequently not
 211 inserted within the atmosphere, which remains dry for all timesteps.

212 3.2. The strength of the turbulent surface exchanges

213 In order to have a wide and controlled variation in \mathcal{F}_f (Eq. 4), we simplify
 214 the representation of the surface fluxes. In PlaSim the temperature tendency
 215 of the first atmospheric layer (of thickness dz) due to the turbulent sensible
 216 heat flux, $(\partial T/\partial t)_{shf}$, is computed as:

$$\left(\frac{\partial T}{\partial t}\right)_{shf} = -\frac{F_T}{\rho c_p dz} = \frac{\gamma_h |\mathbf{u}|}{dz} (T_s - \xi T) = \frac{T_s - \xi T}{\tau_h(\mathbf{x}, t)}, \quad (6)$$

217 in which $F_T = \gamma_h |\mathbf{u}| (T_s - \xi T)$ is the surface sensible heat flux, $\gamma_h = (k/\ln(z/z_0))^2 f(Ri, z_0)$
 218 is the heat transfer coefficients (z is height from the surface, k is the von-
 219 Karman parameter, z_0 is the surface roughness, and f is an empirical func-
 220 tion dependent on stability (as expressed by the Richardson number Ri) and
 221 surface roughness), ξ is the Exner factor (for more details see Louis, 1979;
 222 Lunkeit et al., 2010). The parameter τ_h has time dimension and in a standard
 223 run is a function of space and time, $\tau_h(x, y, z, t) = dz/(\gamma_h(x, y, t)|\mathbf{u}(x, y, t)|)$
 224 but remains of the same order of magnitude. Since we are interested in vari-
 225 ations of orders of magnitude in τ_h , we substitute the locally computed τ_h
 226 with a fixed (in space and time) time scale τ_h as:

$$\left(\frac{\partial T}{\partial t}\right)_{shf} = -\frac{\xi T - T_s}{\tau_h}. \quad (7)$$

227 Similarly to eq. (6), for the wind tendency due to the surface stress, $(\partial \mathbf{u}/\partial t)_{stress}$,
 228 we have:

$$\left(\frac{\partial \mathbf{u}}{\partial t}\right)_{stress} = -\frac{\mathbf{u}}{\tau_m(\mathbf{x}, t)}. \quad (8)$$

229 with $\tau_m(x, y, z, t) = dz/(\gamma_m(x, y, t)|\mathbf{u}(x, y, t)|)$ and the drag coefficient γ_D
 230 defined similarly to γ_h . Again we substitute the locally compute $\tau_m(\mathbf{x}, t)$ with
 231 a fixed (in space and time) drag timescale τ_m (Rayleigh friction timescale).
 232 Generally the drag and heat transfer coefficients γ_D and γ_h – and therefore

233 the time constants τ_m and τ_h – have similar magnitude. This is particularly
 234 true in the case of neutral flows, for which $\gamma_D = \gamma_h$ is indeed a very good
 235 approximation (Arya, 1988; Louis, 1979). For non-neutral flows, γ_h and γ_D
 236 are different but still of the same order of magnitude, as can be seen in Fig.
 237 11.6 of Arya (1988). On the base of this and since in this study we are going
 238 to explore a wide parametric range, we assume for the sake of simplicity:

$$\tau_m = \tau_h = \tau. \quad (9)$$

239 Experiments are performed for $\Omega^* = \Omega/\Omega_E = 1/10, 1/5, 1/2, 1, 2, 4, 8,$
 240 where Ω_E is the Earth rotation rate. For each value of Ω^* we run the model
 241 with $\tau = 2700, 3600, 10800, 21600, 43200, 86400, (86400 \times 3), (86400 \times 10),$
 242 $(86400 \times 30), (86400 \times 100), (86400 \times 500)$ seconds, that is from 45 minutes
 243 (model timestep for $\Omega/\Omega_E \leq 1$) to 500 days. Simulations with very large
 244 τ are representative of an atmosphere with no solid lower boundary (James,
 245 1994; Menou and Rauscher, 2009; Heng et al., 2011b).

246 Let us note that as Ω increases, the typical size of the baroclinic distur-
 247 bances L_c decreases as (Eady, 1949)

$$L_c = 2.4\pi L_R, \quad (10)$$

248 with the Rossby deformation radius $L_R = NH/f$ (James, 1994; Williams,
 249 1988a), N the buoyancy frequency, H the height scale and $f = 2\Omega \sin \varphi$
 250 the Coriolis parameter. For our dry-atmosphere simulations an order-of-
 251 magnitude estimate at the midlatitudes for $\Omega^* = 8$ leads to $\Delta\theta \approx 110$ K,
 252 $\bar{\theta} \approx 240$ K (see, e.g., Fig.3(h)), $\Delta z = 9$ km, $N \approx (g/\bar{\theta}(\Delta\theta/\Delta z))^{1/2} \approx 2 \times 10^{-2}$
 253 s^{-1} and therefore to $L_R \sim 200$ Km. This implies that T42 simulations (spatial
 254 resolution about 250 Km) should be able to capture at least the largest eddies
 255 at $\Omega^* = 8$ and more than adequate for $\Omega^* \leq 4$.

256 4. Circulation regimes at different \mathcal{Ro} and \mathcal{F}_f

257 The diagram in Fig. 1(b) shows the dimensionless space $(\mathcal{F}_f, \mathcal{Ro})$. The
 258 over-plotted bullet points represent numerical experiments performed at $\Omega^* =$
 259 0.1 (circles, denoted as “slow rotation”), $\Omega^* = 1$ (squares, “intermediate ro-
 260 tation”) and $\Omega^* = 8$ (triangles, “fast rotation”) for strong, intermediate and
 261 weak drag condition (τ equal to 45 minutes, 1 day and 500 days respectively)
 262 whose mean meridional and zonal circulations are shown in Fig. 2 and Fig. 3

263 and delimit the portion of the $(\mathcal{F}_f, \mathcal{R}o)$ space covered by the numerical sim-
 264 ulation performed in this study. We have over-plotted the corresponding
 265 values of Ω^* (horizontal dot-dashed lines) and τ (dotted lines) in order to
 266 highlight the connection between the dimensionless numbers and the phys-
 267 ical parameters Ω^* and τ . Note that Ω^* and $\mathcal{R}o$ as well as τ and \mathcal{F}_f point
 268 in opposite directions. In order to help to set the stage for the reader to
 269 understand the results in the following and make it easier to interpret the
 270 montage of figures (3) and (2), we anticipate the main characteristics of the
 271 simulated circulations:

- 272 1. At high thermal Rossby number ($\mathcal{R}o \geq 8$), the decrease of the surface
 273 drag controls the transition from counter- to super-rotating (SR in
 274 Fig.1(a)) equatorial flow. Super-rotation is approached for $\mathcal{F}_f \geq 10^4$;
- 275 2. At intermediate rotation speed ($1 \leq \mathcal{R}o \leq 0.01$), strong drag ($\mathcal{F}_f \leq 10$)
 276 is associated with axisymmetric circulations (AR in Fig. 1(a)). The
 277 decrease of τ leads to the appearance of the indirect Ferrel cell for $10 \leq$
 278 $\mathcal{F}_f \leq 10^5$ characterized by baroclinic activity (BC in Fig.1(a)); further
 279 decrease of the surface drag ($\mathcal{F}_f \geq 10^5$) leads to the emergence of a
 280 barotropic flow (BT in Fig.1(a)) characterised by a large reduction in
 281 the vertical shears of the zonal wind and the the complete disappearing
 282 of the Ferrel cell;
- 283 3. For fast rotations ($\mathcal{R}o \leq 10^{-3}$) the increase the of Taylor frictional
 284 number ($\mathcal{F}_f > 10^4$) leads to the appearance of a multi-jet, zonostrophic
 285 flow (ZN in Fig. 1(a)) for $\mathcal{F}_f > 10^3$ ($\tau > 6$ hours)

286 Boundaries between the different regimes are schematically sketched in Fig.
 287 1(a). In the following we give a detailed description of the different regimes.

288 4.1. *Slow rotation ($\mathcal{R}o = 8$)*

289 Fig. 2(a), 2(b), 2(c) and Fig. 3(a), 3(b), 3(c) show the slow rotation
 290 rate ($\mathcal{R}o = 8$). Such circulations are dominated by one Hadley cell in each
 291 hemisphere which extends northward up to the poles (this regime is denoted
 292 AS in the Fig.1(a)). This is a general consequence of the conservation of
 293 angular momentum and in agreement with the theory of the Hadley circula-
 294 tion of Held and Hou (1980). The temperature features almost no latitudinal
 295 dependence, especially in the middle atmosphere. This is typical of slowly
 296 rotating planets (Williams, 1988a; Navarra and Boccaletti, 2002), and is due

297 to the strong Hadley cell circulation. It is interesting to note the effect
 298 of the surface drag on shaping the Hadley circulation. By comparing Fig.
 299 2(e) to Fig. 2(b) ($\mathcal{R}o, 10^{-1} \rightarrow 8$; $\mathcal{F}_f, 10^3 \rightarrow 10$) and Fig.2(c) to Fig.2(f)
 300 ($\mathcal{R}o, 10^{-1} \rightarrow 8$; $\mathcal{F}_f, 10^7 \rightarrow 10^5$) we note a decrease of the counter-rotating
 301 westward upper-level equatorial jet approaching the beginning of the equa-
 302 torial super-rotation (for example compare Fig 2(c) to Fig. 13 of Heng and
 303 Vogt, 2011). Equatorial super-rotation is indeed expected to take place when
 304 $\mathcal{R}o \gg 1$ (Mitchell and Vallis, 2010). Therefore simulations with $\Omega^* < 1/10$
 305 and moderate or high drag are needed in order to obtain fully super-rotating
 306 atmospheric circulations (as is the case, for example, for Venus to Titan).

307 4.2. Intermediate rotation ($\mathcal{R}o = 0.08$)

308 In the medium rotation case ($\mathcal{R}o = 0.08$), we have atmospheric circula-
 309 tions characterized by strong eastward zonal jets at about $50 - 60^\circ$ and
 310 by a thermally direct (Hadley) and indirect (Ferrel) meridional cell (Fig. 2
 311 (d,e,f) and Fig. 3 (d,e,f)). The general circulation is considerably affected
 312 by the different surface properties. In particular we note that at large \mathcal{F}_f ,
 313 the flow develops strong barotropic horizontal shears, as first discussed by
 314 James and Gray (1986). Note that, as we are considering a dry optically-thin
 315 atmosphere, none of the three circulations shown in Fig. (2(d)-2(f)) is close
 316 to the one we observe on Earth (e.g. Peixoto and Oort (1992)) but rather
 317 similar to that of Mars (Lewis et al., 2010).

318 The effect of the surface drag is particularly evident in the meridional
 319 circulation, which is largely modified by the surface properties. A clear
 320 thermally direct-indirect cell structure emerges in the intermediate cases
 321 $\mathcal{F}_f \sim 10^2$ ($\tau \sim 1$ day), with the boundaries of the Hadley cell at about
 322 40° . The intensity and the extent of the indirect cell is greatly reduced
 323 in the high drag ($\mathcal{F}_f \leq 10^{-1}$) case, when the baroclinic waves are largely
 324 suppressed and the flow tend to become axisymmetric. The Ferrel cell is
 325 instead completely suppressed in the low drag ($\mathcal{F}_f \geq 10^5$) case, where the
 326 flow becomes barotropic. The large impact of the surface properties on the
 327 meridional circulation is related to their impact on the baroclinic distur-
 328 bances (James and Gray, 1986), which normally develop at the edge of the
 329 thermally direct (Hadley) and indirect (Ferrel) cells. The Ferrel cell is re-
 330 lated to the presence of eddy momentum convergence, a key ingredient of
 331 baroclinic disturbances (Holton, 2004), and its disappearance points out the
 332 suppression or weakening of the midlatitude disturbances. In the presence of
 333 weak surface drag, zonal winds tend to have high values at the surface which

334 remain fairly constant with height but change sign at the midlatitudes from
 335 westward to eastward going from the equator to the poles (e.g. Fig. 2(f))
 336 thus generating a strong horizontal shear. Such strong horizontal shears in-
 337 hibit the growth of baroclinic waves, as demonstrated in (James, 1987). On
 338 the other hand, with a surface characterized by a high drag, baroclinicity
 339 is suppressed too, because the system frictional dissipation is too high and
 340 kinetic energy is rapidly extracted not giving eddies the chance to grow and
 341 develop (Kleidon et al., 2003).

342 Let us also note in Fig. 3 the presence of shallow cells embedded close
 343 to the surface embedded in a larger one. This is a characteristic of optically-
 344 thin atmospheres of rocky planets in which the solid lower boundary with low
 345 thermal inertia respond very quickly to diurnal and seasonal solar heating
 346 (Caballero et al., 2008). Similar features are indeed observed in Mars circu-
 347 lation (see e.g. figure 2 of Lewis et al., 2010). Such shallow cells disappears
 348 in fact in the additional runs we have performs at $C_{slab} = 10^8 \text{ JK}^{-1} \text{ m}^{-2}$ (not
 349 shown) and have very little effect on the thermodynamic properties we are
 350 going to discuss in the following sections.

351 4.3. Fast rotation ($\mathcal{R}o = 10^{-3}$)

352 Finally, in the fast rotation runs ($\mathcal{R}o = 10^{-3}$) we observe multiple jets
 353 (Fig. 2(g)-(i)) and multiple meridional cells (Fig. 3(g)-(i)) in agreement with
 354 previous studies (Hunt, 1979; Williams, 1988a) and with the scaling of the
 355 Rossby deformation radius (eq. 10). The decrease of L_R with the rotation
 356 rate makes baroclinic waves less and less efficient in the poleward heat trans-
 357 porting process and reduction of the meridional temperature contrast. The
 358 temperature field in fact shows larger contrast in the meridional and vertical
 359 profile, and the thermal structures tend to be in radiative-convective equi-
 360 librium. The effect of τ is mainly observed in the zonal wind profiles (Fig.
 361 2 (g,h,i)) and in the meridional stream function (Fig. 3(g,h,i)). Multi-jet,
 362 zonostrophic flow (Wang, 2012) emerges as the surface drag decreases for
 363 $\mathcal{F}_f > 10^3$, as can be seen in Fig. 3(i).

364 5. Thermodynamic analysis

365 5.1. Thermodynamic diagnostics

366 The general circulation is the result of the conversion of the available
 367 potential energy generated by radiative differential heating into mechanical
 368 work (winds), as first shown by Lorenz (1955, 1960, 1967). For an atmosphere

369 in a statistical steady state, the rate of generation of available potential
 370 energy, G , the rate of conversion into kinetic energy, W , and the rate of
 371 dissipation of kinetic energy through the turbulent cascade (and ultimately
 372 via viscous dissipation), D , have to be equal when averaged over long time
 373 periods (e.g. a year or longer), $\overline{G} = \overline{W} = \overline{D}$ ($\overline{(\cdot)}$ denotes the time mean).
 374 They are therefore equivalent ways of measuring the strength of the Lorenz
 375 energy cycle (Lorenz, 1955).

376 The energy cycle introduced by Lorenz has been set onto a thermody-
 377 namic framework through the consideration of the effective Carnot engine
 378 describing the ability of the atmosphere to perform work (Johnson, 2000;
 379 Adams and Rennó, 2005; Lucarini, 2009). The atmosphere is seen as a heat
 380 engine which generates mechanical work at average rate \overline{W} from the differen-
 381 tial heating due to radiative and material (e.g. latent heat release) diabatic
 382 processes. If \dot{Q}^+ and \dot{Q}^- are the local positive and negative diabatic heating
 383 rate (i.e. $\dot{Q}^+ = \dot{Q}$ where $\dot{Q} > 0$ and $\dot{Q}^+ = 0$ where $\dot{Q} < 0$ and similarly for
 384 \dot{Q}^-) with

$$\Phi^\pm = \int \dot{Q}^\pm \rho dV, \quad (11)$$

385 we have that $\overline{\Phi^+} + \overline{\Phi^-} = \overline{W} \geq 0$. Moreover, one can define an efficiency η :

$$\eta = \frac{\overline{\Phi^+} + \overline{\Phi^-}}{\overline{\Phi^+}} \quad (12)$$

386 which gives us an indication about the capability of the general circulation
 387 of generating kinetic energy given the net heating input Φ^+ . From Eq. (7)
 388 it follows that

$$\overline{W} = \eta \overline{\Phi^+} \quad (13)$$

389 in full analogy with the definition of efficiency of a heat engine (Fermi, 1956).
 390 Such a quantity has been proved to be particularly relevant in marking the
 391 climatic shifts between the present day climates and the Snowball Earth
 392 (Lucarini et al., 2010; Boschi et al., 2012)

393 Dissipation, and therefore irreversibility, is ubiquitous in planetary atmo-
 394 spheres and, more generally, in nonequilibrium systems. The kinetic energy
 395 of the atmospheric flow is ultimately transferred through a turbulent cascade
 396 to smaller scales where it is then dissipated into heat by friction due to vis-
 397 cosity. Thermal dissipation due to sensible heat fluxes between the surface
 398 and lower atmosphere is another irreversible process which may take place

399 in planetary atmospheres. Planets whose atmospheres allow phase transi-
400 tions of one or more of their chemical substances (e.g. water on Earth or
401 methane on Titan) also experience further irreversible processes as evapo-
402 ration/condensation and diffusion (Goody, 2000; Pauluis and Held, 2002b).
403 Irreversible processes are associated with a positive-defined material entropy
404 production (Peixoto et al., 1991; DeGroot and Mazur, 1984; Kondepudi and
405 Prigogine, 1998; Fraedrich and Lunkeit, 2008; Kleidon, 2009). General dis-
406 cussions about the entropy budget of the climate system and about how to
407 estimate it from climate models can be found in Peixoto et al. (1991), Goody
408 (2000), Kleidon and Lorenz (2005), Kleidon (2009), Pascale et al. (2011a),
409 Pascale et al. (2011b), Lucarini et al. (2011). For a climate with a dry at-
410 mosphere the material entropy production is due to two kinds of processes:
411 dissipation of kinetic energy and sensible heat fluxes. If ϵ^2 is the local rate
412 of kinetic energy dissipation such that $D = \int \epsilon^2 \rho dV$, the entropy production
413 associated with it reads:

$$\dot{S}_{kedis} = \int \frac{\epsilon^2}{T} \rho dV. \quad (14)$$

414 In PlaSim the dissipation of kinetic energy is due to: (i) turbulent stresses in
415 the surface boundary layer (which accounts for more than 50% of the overall
416 dissipation) and, gravity wave drag, implemented as a Rayleigh friction at
417 the highest level with a timescale of 50 days, which we define as D_{phys} .
418 Such contribution to the total mechanical dissipation is diagnosed in the
419 model as $1/2 \int \rho dz (\mathbf{v}_a^2 - \mathbf{v}_b^2)$ where \mathbf{v}_b and \mathbf{v}_a is the velocity before and
420 after the application of the boundary layer scheme and Rayleigh friction;
421 (ii) numerical dissipation due to numerical diffusion of momentum (Johnson,
422 1997), which we call D_{num} . More precisely, in PlaSim horizontal diffusion
423 is implemented by a 8th order hyperdiffusion term applied to the vertical
424 component of the relative vorticity $\zeta = \mathbf{k} \cdot (\nabla \times \mathbf{v})$ and horizontal wind
425 divergence $\delta = \nabla_h \cdot \mathbf{v}$, $\kappa \nabla^8(\zeta, \delta)$, where κ is a coefficient of numerical diffusion
426 – the prognostic equations for the horizontal velocity are transformed into
427 equations for ζ and δ , for more details on PlaSim dynamical core see Lunkeit
428 et al. (2010) –. Although it is hard to interpret D_{num} as representative of
429 small scale dissipative processes (Jablonowski and Williamson, 2011) – the
430 hyperdiffusion schemes do not usually match the symmetry requirements of
431 the stress tensor needed to ensure the conservation of the angular momentum
432 (Becker, 2001) – these contributions are produced by the model and will be
433 taken into account in order to be consistent with the model itself (Johnson,

1997; Egger, 1999; Woollings and Thuburn, 2006). The total dissipation of kinetic energy of the model is therefore $D = D_{phys} + D_{num}$.

Sensible heat in PlaSim is associated with turbulent surface fluxes F_T driven by the temperature difference existing between the lowermost part of the atmosphere and the surface and with numerical vertical and horizontal diffusion (of the same kind of that used for momentum) and dry convection. The material entropy production associated with F_T is:

$$\dot{S}_F = \int F_T \left(\frac{1}{T_a} - \frac{1}{T_S} \right) dA, \quad (15)$$

where T_a is the temperature of the first atmospheric level (where F_T is absorbed thus heating it) and T_S the surface temperature. The material entropy production associated therefore to sensible heat is the sum of the material entropy production due to surface turbulent fluxes, \dot{S}_{sens} and to the other sources of sensible heat (diffusion and dry convection), \dot{S}_{sens} , and it reads

$$\dot{S}_{sens} = \dot{S}_F + \dot{S}_{diff}. \quad (16)$$

The total material entropy production of the system is therefore:

$$\dot{S}_{mat} = \dot{S}_{kedis} + \dot{S}_{sens}. \quad (17)$$

The ratio

$$\alpha = \dot{S}_{sens} / \dot{S}_{kedis} \quad (18)$$

is a measure of the degree of irreversibility of the system, which is zero if all the production of entropy is due to the unavoidable dissipation of the mechanical energy (Lucarini et al., 2010). The parameter α introduced above is related to the Bejan number $\mathcal{B}e$ as $\mathcal{B}e = \alpha + 1$ (Paoletti et al., 1989). Systems with large α are instead characterized by high thermal dissipation relatively to the mechanical viscous dissipation and therefore by a higher degree of irreversibility.

5.2. Dissipative properties of circulation regimes

In this section we analyse the dissipative properties of the different circulations described in Sec. 4 as the parameters Ω and τ , and consequently $\mathcal{R}o$ and \mathcal{F}_f , are varied. Sensitivity studies of dissipative properties have been proposed first by Kunz et al. (2008) and then used extensively in Pascale et al. (2011b) and Boschi et al. (2012) as an insightful way to assess the models' tuning and their thermodynamical properties. In the following, we plot quantities in the (Ω^*, τ) plane for practical purposes, and we overplot the values of $\log_{10} \mathcal{R}o$ and $\log_{10} \mathcal{F}_f$ (Fig. 4 to Fig. 11).

464 *Kinetic energy dissipation and meridional heat transport.* In Fig. 4, the
465 results of the numerical simulations show that for $10^{-2} < \mathcal{R}o < 1$ and
466 $1 < \mathcal{F}_f < 10^3$ there is the highest total dissipation of kinetic energy, D . We
467 observe a non-trivial dependence on Ω and τ . The most intense dissipation
468 is centered around $\mathcal{R}o \approx 0.1$ and $\mathcal{F}_f \approx 10^2$ ($\tau = 12$ hours and $\Omega^* = 1$), with
469 $D \approx 0.45 \text{ W m}^{-2}$. This is mainly associated with the dissipation of kinetic
470 energy in the boundary layer, as can be seen in Fig. 5 where D_{phys} is shown.
471 On the base of the discussion in Section 4, we can speculate that at low val-
472 ues of Ω , the baroclinic eddies become larger than the size of the exoplanet
473 (see equation (10) and related discussion) and thus do not develop; at high
474 values of Ω they become too small, convert inefficiently available potential
475 energy into kinetic energy (Hunt, 1979), and dissipate quickly. Furthermore,
476 the surface properties have a dramatic impact on the circulation, as shown
477 also by James and Gray (1986), because the growth rate of the most unsta-
478 ble baroclinic waves is strongly inhibited by horizontal shears (James, 1987)
479 observed, for example, in Fig. 2(e). This explains the drop of D at high
480 \mathcal{F}_f and intermediate $\mathcal{R}o$. On the other hand, strong drag leads to kinetic
481 energy extraction early in the development of baroclinic eddies. Therefore,
482 the optimal situation is expected for intermediate values of Ω and surface
483 drag. Our results are in agreement with those of Kleidon et al. (2003, 2006),
484 who considered the case $\Omega^* = 1$ only.

485 Moving on to fastly rotating planets, there is a significant decrease of D
486 at low thermal Rossby number ($\mathcal{R}o < 10^{-2}$) for any value of \mathcal{F}_f (zonostrophic
487 flow, ZN). The strength of the Lorenz energy cycle therefore tends to become
488 more insensitive to the surface properties. Interestingly, also circulations of
489 slowly rotating planets with low drag ($\mathcal{R}o > 1$, $\mathcal{F}_f > 10^4$, corresponding
490 with the super-rotation regime, see Fig.1(b)) have very weak kinetic energy
491 dissipation. The dissipation rate remains high for slow rotation and for strong
492 drag ($\mathcal{F}_f \leq 0.1$, $\mathcal{R}o \geq 10$, AS circulations, Fig.1(a)). This is consistent with
493 the fact that in the low rotation, axisymmetric circulations, baroclinicity is
494 mostly absent, and the dissipation of kinetic energy is simply related to the
495 strength of the surface drag, which extracts kinetic energy from the mean
496 flow, thus causing very weak winds near the surface.

497 The meridional heat transport (Peixoto et al., 1991) is in general a very
498 important quantity in planetary atmospheres (Lorenz et al., 2001) and it is
499 associated with the radiative imbalance between high and low temperature
500 regions. The zonal mean of the meridional heat transport $T(\vartheta)$ is worked
501 out at each latitude ϑ by integrating the longitudinally averaged top-of-the-

502 atmosphere (TOA) radiation budget (Lucarini and Ragone, 2011). A scalar
 503 index, MHT , of the meridional heat transport is then defined as half of the
 504 difference of the values of the poleward heat transport in the two hemispheres
 505 at 30° latitude,

$$MHT = 1/2(Tr(\pi/3) - Tr(-\pi/3)). \quad (19)$$

506 MHT thus represents the net heat flowing out of the equatorial region
 507 through zonal walls placed at 30° .

508 Overall we observe that the meridional heat transport increases with $\mathcal{R}o$,
 509 in agreement with the results found in Vallis and Farneti (2009). This general
 510 feature is due to the inefficiency of the too small baroclinic eddies at high Ω
 511 in transporting heat (eq. 10).

512 Furthermore, it is evident that for intermediate rotation rates ($1/5 \leq \Omega^* \leq$
 513 2) MHT peaks at $\tau \approx 1$ day (≈ 1 PW), that is in the region of baroclinic cir-
 514 culations (Fig. 1(b) and 1(a)), coinciding with the maximum in dissipation
 515 (Fig. 4). It is well known in fact that midlatitude eddies constitute a very im-
 516 portant mechanism of meridional heat transport (Lorenz, 1967; James, 1994).
 517 This is also clear from the zonal mean of the transient eddy flux $\overline{v'T'}$ (not
 518 shown), which reaches the highest values ≈ 8 K ms $^{-1}$ at 900 hPa and 50 N/S
 519 for the values of τ maximizing D , compared to 0.5 K ms $^{-1}$ for $\tau = 45$ min
 520 (at 700 hPa and 60 N/S) and 4 K ms $^{-1}$ for $\tau = 500$ days (at 1000 hPa and 50
 521 N/S). Just for the sake of comparison, let us note that for earth's circulation
 522 $\overline{v'T'}|_{max} \approx 15$ K ms $^{-1}$ at 850 hPa and 50 N/S (e.g. James, 1994). In the
 523 slow rotation region ($\mathcal{R}o \approx 10$) we have the largest heat transport (≈ 1.5
 524 PW) at high drag (τ of few hours), which may be explained by lower wind
 525 velocities in the lower branch of the Hadley cell (equatorwards motion).

526 *Efficiency and material entropy production.* The efficiency diagram (Fig. 7)
 527 shows that the highest value of η lay in the intermediate rotation range with
 528 values of $\approx 3\%$ in correspondence of the baroclinic and axisymmetric cir-
 529 culations. At low rotations, the high-drag circulations ($\mathcal{F}_f < 1$) are the most
 530 efficient. Interestingly, we note that circulations tending toward equatorial
 531 super-rotation have a quite substantial drop in efficiency which reduces to
 532 $\approx 1\%$. At low $\mathcal{R}o$ the thermodynamic efficiency drops below 1% because of
 533 the drastic drop in D associated with the weakening of the Lorenz energy
 534 cycle, therefore zonostrophic flows are very inefficient circulation regimes in
 535 terms of converting heat into mechanical work. Let us note that although we
 536 are dealing with a dry atmosphere, and therefore very different from a moist
 537 one (in which the magnitude of the heat losses and gain is much higher,

538 for example the latent heat gives a positive heating contribution of ~ 80
 539 W m^{-2}), η has comparable values (see e.g. Lucarini et al., 2010) and does
 540 not generally exceeds 3%.

541 The material entropy production terms (eq. (14, 16 and 17)) are shown
 542 in Fig. 8-10. Fig. 8 shows the contribution due to thermal dissipation \dot{S}_{sens}
 543 (15). This is dominated by \dot{S}_F , which accounts for almost 2/3 of \dot{S}_{sens} and is
 544 almost independent from \mathcal{Ro} , having its highest values for $\tau \sim 3$ days. Such
 545 a pattern is explained by a trade-off mechanism between the sensible heat
 546 flux, which decreases with τ independently at any \mathcal{Ro} (not shown), and the
 547 temperature difference between the surface and the near-surface atmosphere,
 548 which increases with τ since, due to eq. (7), surface and atmospheres tend to
 549 be more decoupled. The entropy production associated with the dissipation
 550 of kinetic energy, \dot{S}_{kedi} (Fig. 9) closely follows the pattern of D (Fig. 4) as
 551 evident from its own definition (eq. (14)).

552 The total material entropy production (17) is the sum of the two, so
 553 its properties are determined mainly by \dot{S}_{sens} which is generally larger than
 554 \dot{S}_{kedi} ($\sim 1-2$ times in the at low-intermediate rotation rates, as can be seen
 555 in Fig. 11 where the irreversibility parameter α is shown, and up to 10 times
 556 for fast rotating planets). The region of highest material entropy production
 557 ($\approx 3.5 \text{ mW m}^{-2} \text{ K}^{-1}$) is observed for $0.1 \leq \mathcal{Ro} \leq 0.01$ and $10^2 \leq \mathcal{F}_f \leq 10^3$,
 558 and generally the whole region of the diagram in Fig. 1(b) with $0.5 \text{ day} \leq \tau \leq$
 559 5 days have large material entropy production. Overall, the material entropy
 560 production tends to be fairly low ($\approx 1.5 \text{ mW m}^{-2} \text{ K}^{-1}$) for fast rotation speeds
 561 (e.g. $\mathcal{Ro} \sim 10^{-3}$) where we have very low values of \dot{S}_{sense} and lower values of
 562 \dot{S}_{kedi} . Let us note that the portion of the diagram corresponding to super-
 563 rotating fluids (SR in Fig. 1(a)) is characterized by very low mechanical and
 564 thermal dissipation and therefore very low material entropy production. In
 565 this respect super-rotating flows are quite interesting since such circulations
 566 are also characterized by very low efficiency. In other terms they seem to
 567 have a behavior close to inviscid, non-dissipative fluids (for which $D = 0$
 568 and $\dot{S}_{sens} = 0$ by definition). Mitchell and Vallis (2010) also pointed out
 569 some peculiar dynamical properties of super-rotating flows, as for example
 570 the fact that the equatorial, strong eastwards jet, once established, do not
 571 need eddy-forcing to be maintained. Interestingly, these results make clear
 572 that there is no obvious correspondence between the presence of large amount
 573 of kinetic energy in the atmosphere and the presence of an intense Lorenz
 574 energy cycle to support its generation. This matter has been hotly debated
 575 in a rather different scientific context, where the possibility of extracting

576 massive amounts of energy from the atmospheric circulation by wind turbines
577 is discussed (Miller et al., 2011).

578 A schematic diagram summarising the main thermodynamical properties
579 discussed so far for the different circulation regimes is shown in Fig. 1(b):

- 580 1. Baroclinic regime (BC): high D , high η , relatively high MHT ;
- 581 2. Super-rotation (SR): low D , low η , low \dot{S}_{mat} ;
- 582 3. Zonostrophic flow (ZN): low D , low MHT , low η ;
- 583 4. Axisymmetric flow (AS): high MHT and D for $\mathcal{R}o > 1$, high η for
584 $1 < \mathcal{R}o < 0.1$, low D , MHT and η for $\mathcal{R}o < 0.01$.

585 5.3. Implications for the Maximum Entropy Production Principle

586 In this section we briefly describe our results in the context of the Max-
587 imum Entropy Production Principle (MEPP, Paltridge, 1975, 1978, 2001),
588 as this conjecture has gained some momentum also in the planetary science
589 community (Lorenz et al., 2001; Taylor, 2010). MEPP has been used as
590 a closure condition for climatic toy-models (Lorenz et al., 2001) or simple
591 energy balance climate models (e.g. Paltridge, 1975) in order to determine
592 dynamical quantities as the meridional heat transport. A further, possible
593 application was shown by Kleidon et al. (2003) and Kunz et al. (2008), who
594 suggested to use MEPP as a guide for tuning sub-grid motion parameters of
595 PUMA, an atmospheric general circulation models (Fraedrich et al., 2005).
596 For example, let us consider the Rayleigh drag constant τ (eq. 6 and following
597 discussion) depends on the drag coefficient γ_h which in turn depends on both
598 surface roughness and dynamical quantities. Therefore different values of τ
599 can be thought of associated with either different surface properties (as done
600 in the rest of the paper) or to different strengths of the turbulent transfer in
601 the planetary boundary layer. Following the second interpretation, Kleidon
602 et al. (2003) showed that the value of τ giving the most realistic atmospheric
603 state was that maximizing the entropy production of the system. However,
604 one major criticism that MEPP has encountered is that it does not take into
605 account the effects of the rotation speed (Rodgers, 1976; Goody, 2007; Jupp
606 and Cox, 2010). This was related to the criticisms on whether one could
607 use MEPP to infer the meridional energy transport. In this study we are
608 in a position to have a broader look on the results of Kleidon et al. (2003)
609 since a more detailed diagnostics for the dissipative properties and a larger

610 dynamical range for atmospheric circulations are available. Of course our
 611 aim is not, and we do not claim, to prove or disprove MEPP, for which a
 612 rigorous demonstration is still missing (Dewar, 2005; Grinstein and Linsker,
 613 2007).

614 In order to test MEPP, we perform control runs in which the full bound-
 615 ary layer scheme (Louis, 1979; Louis et al., 1981) is employed without the
 616 simplification of Sect. 3.2 (so τ is not prescribed but dynamically determined
 617 depending on the winds and vertical stability). In the following we shall re-
 618 fer to them and to quantities evaluated for such simulations with the label
 619 “BLS” (boundary layer scheme). In BLS simulations the drag coefficient is
 620 consistently determined at each timestep and each grid-point according to the
 621 Monin-Obukhov theory (e.g. Arya, 1988) and not prescribed as a constant
 622 parameter. Since this set up employes a more refined and realistic represen-
 623 tation of the boundary layer physics, we consider it as our “reality” towards
 624 which comparing simulations in which the rougher, tunable τ -scheme is used.
 625 Zonal means of the BLS simulations are shown in Fig. 13 – cross sections of
 626 temperature and zonal winds – and in Fig.14 – meridional streamfunctions –
 627 for simulations for $\Omega^* = 1/10, 1, 8$ respectively. For each Ω^* , we consider τ as
 628 a tunable parameter and select the value $\tau_{max}(\Omega^*)$ maximising \dot{S}_{mat} (which
 629 can be easily visualized in Fig. 10). Furthermore, we take into account also
 630 $\dot{S}_{kedi\text{ss}}$ (Fig. 9), so that we can be informative also on the maximum dissi-
 631 pation principle (Lorenz, 1967; Ozawa et al., 2003; Schulman, 1977; Pascale
 632 et al., 2011b). We denote with $\tilde{\tau}_{max}(\Omega^*)$ the values of τ maximising $\dot{S}_{kedi\text{ss}}$.
 633 As can be seen in Fig. 9-10, τ_{max} and $\tilde{\tau}_{max}$ differ mostly for $\Omega^* \leq 1/2$ (where
 634 the maximum dissipation steady states occur for τ of few hours) whereas
 635 they are mostly the same (1 day) for $\Omega^* > 2$ days ($\tau \approx 1$ day).

636 In Fig. 12(a) and 12(b) we compare $\dot{S}_{mat}(\Omega^*; \tau_{max})$ and $\dot{S}_{kedi\text{ss}}(\Omega^*; \tau_{max})$
 637 (dashed line) with $\dot{S}_{mat}^{BLS}(\Omega^*)$ and $\dot{S}_{kedi\text{ss}}^{BLS}(\Omega^*)$ respectively (continuous lines).
 638 On the same diagrams we also show the same quantities for $\tau = 0.1 \tau_{max}(\Omega^*)$
 639 (dotted line) and $\tau = 10 \tau_{max}(\Omega^*)$ (dotted-dashed line) in order to provide
 640 an indication of the sensitivity of \dot{S}_{mat} and $\dot{S}_{kedi\text{ss}}$ with respect to τ_{max} . The
 641 MEPP estimate of \dot{S}_{mat} slightly overestimate the values obtained in controls
 642 runs ($\leq 5\%$) but, impressively, captures fairly well the dependence on Ω^* .
 643 Similarly, the values of $\dot{S}_{kedi\text{ss}}$ obtained for τ_{max} compare relatively well with
 644 the ones obtained in the controls runs. Circulations corresponding to τ_{max}
 645 are indeed fairly similar to BLS circulations, as can be seen by comparing
 646 Fig. 13(a,b,c) with Fig. 2(b,e,h) and Fig. 14(a,b,c) with Fig. 3(b,e,h).

647 When the values of $\tilde{\tau}_{max}(\Omega^*)$ associated with the maximum of $\dot{S}_{kedi\text{ss}}$ is

648 instead taken into account (Fig. 12(c)-12(d)), we observe that $\dot{S}_{mat}(\Omega^*, \tilde{\tau}_{max})$
649 provides again a quite good estimate of \dot{S}_{mat}^{BLS} , with a slight underestimate
650 ($\approx 9\%$) for $\Omega^* < 1/2$, due to the fact that for such values of the rotation
651 rate $\tilde{\tau}_{max}$ bends towards smaller τ where \dot{S}_{mat} tends to decrease (Fig. 10).
652 More unsatisfactory is $\dot{S}_{kedis}(\Omega^*, \tilde{\tau}_{max})$ again for $\Omega^* < 1/2$, with a difference
653 of about 16% with respect to \dot{S}_{kedis}^{BLS} .

654 In the end, both maximum entropy production and maximum dissipa-
655 tion principle provide fairly reasonable estimates of \dot{S}_{kedis}^{BLS} and \dot{S}_{mat}^{BLS} , with
656 the maximum entropy production one having better skills at low Ω^* . The
657 quasi-equivalence of the the two methods is due to the fact that, for such
658 simulations, both \dot{S}_{mat} and \dot{S}_{kedis} have their maxima in the (Ω^*, τ) almost in
659 the same regions. These results seem to confirm, in a relatively large range
660 of dynamical regimes, the possibility of using MEPP in its weak form, as a
661 guide for tuning sub grid parameters associated with turbulent motions, as
662 indicated by Kleidon et al. (2003).

663 6. Conclusions

664 Stimulated by the ongoing development of exoplanet sciences, in this
665 study we have investigated the nonequilibrium thermodynamic properties
666 (kinetic energy dissipation, material entropy production, efficiency, merid-
667 ional heat transport) of optically-thin, non-condensing planetary atmospheres
668 at different values of the thermal Rossby number \mathcal{Ro} and the Taylor number
669 \mathcal{F}_f through a systematic variation of the rotation rate Ω and surface drag
670 time constant τ . The most relevant achievement of this study has been the
671 characterization of the nonequilibrium properties of the different circulation
672 regimes (axisymmetric, super-rotation, baroclinic, barotropic, zonostrophic)
673 obtained with numerical simulations with some interesting connection to the
674 Maximum Entropy Production Principle (MEPP).

675 Slowly rotating planets ($\mathcal{Ro} > 1$) circulation are mostly Hadley cell-
676 dominated but tend to equator; super-rotation for $\mathcal{F}_f > 10^5$. For interme-
677 diate rotation rates ($1 < \mathcal{Ro} < 0.01$) an axisymmetric ($\mathcal{F}_f < 10$), baroclinic
678 ($10 < \mathcal{F}_f < 10^5$) and barotropic ($\mathcal{F}_f > 10^5$) regime are found. At high
679 rotation rates ($\mathcal{Ro} < 0.01$) circulations are characterized by multiple jets
680 (zonostrophic) for $\mathcal{F}_f > 10^4$.

681 The baroclinic regime has high values of D and MHT since midlatitude
682 baroclinic waves provide a very effective way to convert available potential
683 energy into mechanical kinetic energy and transport energy from low to high

684 latitudes. Such mechanism is inhibited by strong barotropic shears charac-
685 terizing the barotropic regime and therefore both D and MHT experience
686 lower values. The axisymmetric regime has different thermodynamic prop-
687 erties depending on the value of $\mathcal{R}o$ at which it is realised. For $\mathcal{R}o > 1$,
688 a very intense Hadley cell develops associated with high MHT and D ; for
689 $1 < \mathcal{R}o < 0.1$ such quantities are weaker but circulations are more efficient
690 in converting heat into mechanical work (high η); at faster rotation speeds
691 ($\mathcal{R}o < 0.01$) a dramatic drop in D , MHT and η is observed. A very in-
692 teresting case is that of circulation approaching equatorial super-rotation
693 ($\mathcal{R}o \leq 10$, $\mathcal{F}_f > 10^5$), for which low D , low η , low \dot{S}_{mat} occurs, thus show-
694 ing a behavior close to inviscid, non-dissipative fluids (for which $D = 0$ and
695 $\dot{S}_{sens} = 0$ by definition). Zonostrophic flows low, typical of fast rotating,
696 low surface drag planets, have a very weak atmospheric energy cycle (low
697 D), are very inefficient in converting potential energy into work and have
698 very low meridional heat transport MHT , therefore showing a temperaure
699 profile close to the radiative-convective equilibrium (which by definition has
700 $MHT = 0$).

701 The thermal dissipation \dot{S}_{sens} is instead fairly insensitive to $\mathcal{R}o$ and is
702 determined mainly by the timeconstant τ , due to a trade-off mechanism
703 between the temperature difference and the heat flux.

704 Moreover, we have shown that the possibility of applying MEPP in its
705 weak form, e.g. as a tool for providing guidance in tuning subgrid scale, seems
706 to work relatively well in the range of values of the rotation rate considered in
707 this study, thus extending the results obtained by Kleidon et al. (2003) when
708 considering the terrestrial rotation rate only. Interestingly, there is broad
709 agreement between what prescribed by applying MEPP and the maximum
710 dissipation principle.

711 This is a first preliminary study for a special case of dry atmosphere. The
712 presence of the hydrological cycle has a huge effect on the circulation and
713 on the energetics and would be definitely worth investigating. Another issue
714 is the role of the surface heat capacity, which would also deserve a system-
715 atic investigation. Furthermore, thermodynamic and dynamical properties
716 of slowly rotating planets, e.g. from $\Omega^* = 1/10$ up to phase-locked planets,
717 are still poorly known and would deserve more investigation too.

718 *Acknowledgments.* The authors thank S. Ehrenreich, K. Fraedrich, N. Iro, E.
719 Kirk, J. Lloyd, F. Lunkeit, R. Plant and P. Read for their helpful and useful
720 comments. This work was supported by the EU-FP7 ERC grant NAMASTE.

721 SP, VL, FR and RB acknowledge the support of CLISAP. We thank the two
722 anonymous referees for their insightful comments which lead to a significant
723 improvement of the manuscript.

724 **References**

725 Burrows, A. et al., 1997. A nongray theory of extrasolar giant planets and
726 brown dwarfs. *The Astrophysical Journal* **491**, 856–875.

727 Arya, S. P., 1988. *Introduction to Micrometeorology*. Academic Press.

728 Donohoe, A. and Battisti D. S., 2012. What determines meridional heat
729 transport in climate models? *Journal of Climate* **25**, 3832 – 3850.

730 Becker, E., 2001. Symmetric stress tensor formulation of horizontal momen-
731 tum diffusion in a global model of atmospheric circulation. *Journal of At-
732 mospheric Sciences* **58**, 269–282.

733 Berger, A., 1978. Long-term variations of daily insolation and quaternary
734 climatic change. *J. Atmos. Sci.* **35**, 2362-2367

735 Bonfils, X. et al., 2012. The HARPS search for southern extra-solar planets
736 XXXI. the m-dwarf sample. *Astronomy and Astrophysics*, in press.

737 Boruck, W. and coauthors, 2011. Characteristics of Planetary Candidates
738 Observed by Kepler. II. Analysis of the First Four Months of Data *The
739 Astrophysical Journal* **736**, 19.

740 Boschi, R., Lucarini, V., Pascale, S., 2012. Bistability of the cli-
741 mate around the habitable zone: a thermodynamic investigation.
742 <http://arxiv.org/abs/1207.1254>.

743 Budyko, M. I., 1969. The effect of solar radiation variations on the climate
744 of the Earth. *Tellus* **5**, 611-619.

745 Caballero et al., 2008. Axisymmetric, nearly inviscid circulations in non-
746 condensing radiative-convective atmospheres. *Quarterly Journal of the
747 Royal Meteorological Society* **134**, 1269–1285.

748 Charbonneau et al., 2009. A super-Earth transiting a nearby low-mass star.
749 *Nature* **462**, 891–894.

- 750 Clancy et al., 2007. Dynamics of the venus upper atmosphere: global-
751 temporal distribution of winds, temperature, and CO at the Venus
752 mesopause. *Bull. Am. Astron. Soc.* **39**, 539.
- 753 Dahms, E., Lunkeit, F., Fraedrich, K., 2012. Low-frequency climate variabil-
754 ity of an aquaplanet. *J. Clim.*, submitted.
- 755 DeGroot, S., Mazur, P., 1984. *Non-equilibrium thermodynamics*. Dover.
- 756 Dewar, R. C., 2005. Maximum entropy production and the fluctuation theo-
757 rem. *Journal of Physics A* **38**, L371–L381.
- 758 Dobbs-Dixon, I., Agol, E., and Burrows, A., 2012. The Impact of Circum-
759 planetary Jets on Transit Spectra and Timing Offsets for Hot Jupiters. *The*
760 *Astrophysical Journal* **751**, 87
- 761 Dvorak, R., 2008. *Extrasolar Planets*. Wiley-VHC.
- 762 Eady, E., 1949. Long waves and cyclone waves. *Tellus* **1**, 33–52.
- 763 Egger, J., 1999. Numerical generation of entropies. *Monthly Weather Review*
764 **127**, 2211–2216.
- 765 Eliassen, E., Machenhauer, B., Rasmussen, E., 1970. On a numerical method
766 for integration of the hydrodynamical equations with a spectral representa-
767 tion of the horizontal fields. Report no. 2, Inst. of Theor. Met., University
768 of Copenhagen.
- 769 Fermi, E., 1956. *Thermodynamics*. Dover.
- 770 Fraedrich, K., Jansen, H., Kirk, E., Luksch, U., Lunkeit, F., 2005. The planet
771 simulator: towards a user friendly model. *Meteorologische Zeitschrift*
772 **14** (3), 299–304.
- 773 Fraedrich, K., Lunkeit, F., 2008. Diagnosing the entropy budget of a climate
774 model. *Tellus A* **60** (5), 921–931.
- 775 Fraedrich, K., E. Kirk, U. Luksch, and F. Lunkeit, 2005. The Portable Uni-
776 versity Model of the Atmosphere (PUMA): Storm track dynamics and low
777 frequency variability. *Meteorol. Zeitschrift* **14**, 735-745.

- 778 Frierson, D. M. W., Held I. M., Zurita-Gotor, P., 2006. A gray-radiation
779 aquaplanet moist GCM. Part I: static stability and eddy scale. *J. Atmos.*
780 *Sci.* **63**, 2548–2566
- 781 Gallavotti, G., 2006. *Encyclopedia of mathematical physics*. Elsevier, Ch.
782 Nonequilibrium statistical mechanics (stationary): overview, pp. 530–539.
- 783 Geisler, J. E., Pitcher, E. J., Malone, R. C., 1983. Rotating-fluid experiments
784 with an atmospheric general circulation model. *Journal of Geophysical*
785 *Research* **88** (C14), 9706–9716.
- 786 Genio, A. D., Suozzo, R., 1987. A comparative study of rapidly and slowly
787 rotating regimes in a terrestrial general circulation model. *J. Atmos. Sci.*
788 **44**, 973–986.
- 789 Goody, R., 2000. Sources and sinks of climate entropy. *Quarterly Journal of*
790 *the Royal Meteorological Society* **126**, 1953–1970.
- 791 Goody, R., 2007. Maximum entropy production in climate theory. *Journal of*
792 *the Atmospheric Sciences* **64**, 2735–2739.
- 793 Grinstein, G., Linsker, R., 2007. Comments on a derivation and application
794 of the maximum entropy production principle. *J. Phys A* **40**, 9717–9720.
- 795 Held, I. M., Hou, A. Y., 1980. Nonlinear axially symmetric circulations in a
796 nearly inviscid atmosphere. *Journal of Atmospheric Sciences* **37**, 515–533.
- 797 Heng, K., 2012. The study of climates of alien worlds. *American Scientist*
798 **100** (4), 334–341, arXiv: 1206.3640
- 799 Heng, K., Frierson, D. M., Phillipps, P. J., 2011a. Atmospheric circulation
800 of tidally locked exoplanets: II dual-band radiative transfer and convec-
801 tive adjustment. *Monthly Notices of the Royal Astronomical Society* **420**,
802 2669–2696.
- 803 Heng, K., Menou, K., Phillips, P. J., 2011b. Atmospheric circulation of
804 tidally locked exoplanets: a suite of benchmark tests for dynamical solvers.
805 *Monthly Notices of the Royal Astronomical Society* **413**, 2380–2402.
- 806 Heng, K. and Vogt, S. S., 2011. Gliese 581g as a scaled-up version of Earth:
807 atmospheric circulation simulations. *Mon. Not. R. Astron. Soc.* **415**, 2145.

- 808 Hide, R., 1953. Some experiments on thermal convection in a rotating liquid.
809 Q. J. R. Meteorol. Soc. **79**, 161.
- 810 Hide, R., 1969. Some laboratory experiments on free thermal convection in
811 a rotating fluid subject to a horizontal temperature gradient and their
812 relation to the theory of the global atmospheric circulation. Corby, G.A.
813 (Ed.), *The Global Circulation of the Atmosphere*, Royal Meteorological
814 Society, London, 196–221.
- 815 Hide, R., 2010. A path of discovery in geophysics fluid dynamics. *Astronomy
816 and Geophysics* **51** (4), 16–23.
- 817 Hide, R., Mason, P., 1975. Some experiments on thermal convection in a
818 rotating liquid. *Adv. Phys.* **24**, 47–99.
- 819 Holton, J. R., 2004. *An introduction to Dynamic Meteorology*. Elsevier Aca-
820 demic Press.
- 821 Hourdin, F., O. et al. 1995. Numerical simulations of the general circulations
822 of the atmosphere of Titan. *Icarus* **117**, 358–374.
- 823 Hunt, B., 1979. The influence of the earth’s rotation rate on the general
824 circulation of the atmosphere. *J. Atmos. Sci.* **36**, 1392–1408.
- 825 Jablonowski, C., Williamson, D., 2011. Numerical techniques for global at-
826 mospheric models. Springer, Ch. The pros and cons of diffusion, filters and
827 fixers in atmospheric general circulation models, pp. 381–493.
- 828 James, I., 1994. *Introduction to Circulating Atmosphere*. Cambridge Univer-
829 sity Press.
- 830 James, I., Gray, L., 1986. Concerning the effect of surface drag on the circu-
831 lation of a baroclinic planetary atmosphere. *Quart. J. R. Met. Soc.* **112**,
832 1231–1250.
- 833 James, I. N., 1987. Suppression of baroclinic instability in horizontal sheared
834 flows. *Journal of Atmospheric Sciences* **44** (24), 3710–3720.
- 835 Johnson, D., 1997. ”General coldness of climate” and the second law: Impli-
836 cations for modelling the earth system. *Journal of Climate* **10**, 2826–2846.

- 837 Johnson, D. R., 2000. General Circulation Model Development: Past, Present
838 and Future. Accademic Press, New York, Ch. Entropy, the Lorenz Energy
839 Cycle and Climate, pp. 659–720.
- 840 Joshi, M. M., 2003. Climate model studies of synchronously rotating planets
841 *Astrobiology* **3**(2), 415–27, PMID 14577888
- 842 Jupp, T., Cox, P., 2010. MEP and planetary climates: insights from a two-
843 box climate model containing atmospheric dynamics. *Philosophical Trans-*
844 *actions of the Royal Society B* **365**, 1355–1365.
- 845 Kleidon, A., 2009. Nonequilibrium thermodynamics and maximum entropy
846 production in the earth system. *Naturwissenschaften* **96**, 653–677.
- 847 Kleidon, A., Fraedrich, K., Kirk, E., Lunkeit, F., 2006. Maximum en-
848 tropy production and the strenght of boundary layer exchange in an at-
849 mospheric general circulation model. *Geophysical Research Letters* **33**,
850 doi:10.1029/2005GL025373.
- 851 Kleidon, A., Fraedrich, K., Kunz, T., Lunkeit, F., 2003. The atmospheric
852 circulation and the states of maximum entropy production. *Geophysical*
853 *Research Letters* **30** (23), doi:10.1029/2003GL018363.
- 854 Kleidon, A., Lorenz, R., 2005. Non-equilibrium Thermodynamics and the
855 Production of Entropy. *Understanding Complex Systems*. Springer, Berlin.
- 856 Kondepudi, D., Prigogine, I., 1998. *Modern Thermodynamics: From Heat*
857 *Engines to Dissipative Structure*. John Wiley, Hoboken, N.J.
- 858 Kundu, P., Cohen, I. M., 2004. *Fluid Mechanics*. Accademic Press.
- 859 Kunz, T., Fraedrich, K., Kirk, E., 2008. Optimisation of simplified GCMs
860 using circulation indices and maximum entropy production. *Climate Dy-*
861 *namics* **30**, 803–813.
- 862 Kuo, H., 1965. On formation and intensification of tropical cyclones through
863 latent heat release by cumulus convection. *J. Atmos. Sci.* **22**, 40–63.
- 864 Kuo, H., 1974. Further studies of the parametrisation of the influence of
865 cumulus convection on large-scale flow. *J. Atmos. Sci.* **31**, 1232–1240.

- 866 Lacis, A., Hansen, K., 1974. A parametrisation for the absorption of solar
867 radiation in the earth's atmosphere. *J. Atmos. Sci.* **31**, 118–133.
- 868 Laursen, L., Eliassen, E., 1989. On the effect of the damping mechanisms in
869 an atmospheric general circulation model. *Tellus* **41A**, 385–400.
- 870 Lewis N. K. et al., 2010. Atmospheric circulation of eccentric hot nep-
871 tune GJ436b. *The Astrophysical Journal* **720**, 344, doi:10.1088/0004-
872 637X/720/1/344.
- 873 Lorenz, E., 1955. Available potential energy and the maintenance of the
874 general circulation. *Tellus* **7**, 271–281.
- 875 Lorenz, E., 1960. Generation of available potential energy and the intensity
876 of the general circulation. Pergamon, Tarrytown, N.Y.
- 877 Lorenz, E., 1967. The nature and theory of the general circulation of the
878 atmosphere. Vol. 218.TP.115. World Meteorological Organization.
- 879 Lorenz, R., Lunine, J., Withers, P., McKay, C., 2001. Titan, Mars and Earth:
880 Entropy production by latitudinal heat transport. *Geophysical Research*
881 *Letters* **28** (3), 415–418.
- 882 Louis, J., 1979. A parametric model of vertical eddy fluxes in the atmosphere.
883 *Bound. Layer Meteorol.*, 187–202.
- 884 Louis, J., Tiedke, M., Geleyn, J., 1981. A short history of the pbl parametri-
885 sation at ecmwf. Proceedings of the ECMWF Workshop on Planetary
886 Boundary Layer Parametrization, 59–80.
- 887 Lucarini, V., 2009. Thermodynamic efficiency and entropy produc-
888 tion in the climate system. *Physical Review E* **80**, 021118,
889 doi:10.1103/PhysRevE.80.02118.
- 890 Lucarini, V., 2012. Modelling complexity: the case of climate science.
891 arXiv:1106.1265v1 [physics.hist-ph]; in press, Proceedings of the Confer-
892 ence "Models, Simulation and the Reduction of Complexity", De Gruyter
893 Verlag, Hamburg.
- 894 Lucarini, V., Ragone, F., 2011. Energetics of Climate Models: Net Energy
895 Balance and Meridional Enthalpy Transport. *Reviews of Geophysics* **49**,
896 RG1001, doi:10.1029/2009RG000323.

- 897 Lucarini, V., Fraedrich, K., Lunkeit, F., 2010. Thermodynamic analysis of
898 snowball earth hysteresis experiment: efficiency, entropy production and
899 irreversibility. *Quarterly Journal of Royal Meteorological Society* **136**, 1–
900 11.
- 901 Lucarini, V., Fraedrich, K., Ragone, F., 2011. New results on the thermody-
902 namic properties of the climate. *Journal of the Atmospheric Sciences* **68**,
903 2438–2458.
- 904 Lunkeit, F., Borth, H., Böttinger, M., Fraedrich, K., Jansen, H., Kirk, E.,
905 Kleidon, A., Luksch, U., Paiewonsky, P., Schubert, S., Sielmann, S., Wan,
906 H., 2010. Planet simulator, reference manual (version 16). Tech. rep., Uni-
907 versity of Hamburg, www.mi.uni-hamburg.de/Downloads-un.245.0.html.
- 908 Menou, K., Rauscher, E., 2009. Atmospheric circulations of hot jupiters: a
909 shallow three dimensional model. *The Astrophysical Journal* **700**, 887–897.
- 910 Merlis, T. M. and Schneider, T., 2010. Atmospheric dynamics of Earth-like
911 tidally locked aquaplanets. *Journal of Advances in Modeling Earth Sys-*
912 *tems*, **2** (13), 17 pp.
- 913 Miller L. M., Gans F., Kleidon A., 2011. Jet stream wind power as a re-
914 newable energy resource: little power, big impacts. *Earth Syst. Dynam.* **2**,
915 201-212.
- 916 Mitchell, J. L. and Vallis, G. K., 2010. The transition to superrotation in
917 terrestrial atmospheres. *Journal of Geophysical Research*, **115** E12008,
918 doi:10.1029/2010JE003587.
- 919 Navarra, A., Boccaletti, C., 2002. Numerical general circulation experiments
920 of sensitivity to earth rotation rate. *Climate Dynamics* **19**, 467–483.
- 921 Orszag, S., 1970. Transform method for the calculation of vector coupled
922 sums. *J. Atmos. Sci.*, 890–895.
- 923 Ozawa H, Ohmura A, Lorenz R. D., Pujol T., (2003). The second law of
924 thermodynamics and the global climate system: A review of the maximum
925 entropy production principle. *Reviews of Geophysics* **41** 1018, 2003 (doi:
926 10.1029/2002RG000113)

- 927 Paltridge, G. W., 1975. Global dynamics and climate—a system of minimum
928 entropy exchange. *Quarterly Journal of the Royal Meteorological Society*
929 **101**, 475–484.
- 930 Paltridge, G. W., 1978. The steady state format of global climate. *Quarterly*
931 *Journal of Royal Meteorological Society* **104**, 927–945.
- 932 Paltridge, G. W., 2001. A physical basis for a maximum of thermodynamic
933 dissipation of the climate system. *Quarterly Journal of the Royal Meteorological Society* **127**, 305–313.
- 935 Paoletti, S., Rispoli, F., Sciubba, E., 1989. Calculation of exergetic losses in
936 compact heat exchanger passages. *ASME AES* **10** (2), 21–29.
- 937 Pascale, S., Gregory, J., Ambaum, M., Tailleux, R., 2011a. Climate entropy
938 budget of the HadCM3 atmosphere-ocean general circulation model and
939 FAMOUS, its low-resolution version. *Climate Dynamics* **36** (5-6), 1189–
940 1206.
- 941 Pascale, S., Gregory, J., Ambaum, M., Tailleux, R., 2011b. A parametric
942 sensitivity study of entropy production and kinetic energy dissipation us-
943 ing the FAMOUS AOGCM. *Climate Dynamics*, doi 10.1007/s00382-011-
944 0996-2.
- 945 Pauluis, O., Held, M., 2002a. Entropy budget of an atmosphere in radiative-
946 convective equilibrium. Part I: Maximum work and frictional dissipation.
947 *Journal of the Atmospheric Sciences* **59**, 125–139.
- 948 Pauluis, O., Held, M., 2002b. Entropy budget of an atmosphere in radiative-
949 convective equilibrium. Part II: Latent heat transport and moist processes.
950 *Journal of the Atmospheric Sciences* **59**, 140–149.
- 951 Peixoto, J., Oort, A., de Almeida, M., Tomé, A., 1991. Entropy budget of
952 the atmosphere. *Journal of Geophysical Research* **96**, 10981–10988.
- 953 Peixoto, J. P., Oort, A., 1992. *Physics of the Climate*. Springer-Verlag, New
954 York.
- 955 Pierrehumbert, R. T., A Palette of Climates for Gliese 581g. *The Astrophysical Journal Letters* **726** (1), L8.

- 957 Rauscher E. and Menou, K., 2012. The role of drag in the energet-
958 ics of strongly forced exoplanets. *The Astrophysical Journal* **745**, 78
959 doi:10.1088/0004-637X/745/1/78
- 960 Read, P., 2001. Transition to geostrophic turbulence in the laboratory, and
961 as a paradigm in atmospheres. *Surveys Geophys.* **22**, 231–249.
- 962 Read, P., 2011. Dynamic and circulation regimes of terrestrial planets. *Plan-*
963 *etary and space sciences* **59**, 900–914.
- 964 Read, P., Collins, M., Früh, W.-G., Lewis, S., Lovegrove, A., 1998. Wave
965 interactions and baroclinic chaos: a paradigm for long timescale variability
966 in planetary atmospheres. *Chaos Solitons Fractals* **9**, 1221–1227.
- 967 Adams, D., K., Rennó, N., O., 2005. Thermodynamic efficiencies of an ide-
968 alized global climate model. *Climate Dynamics* **25**, 801–813.
- 969 Rodgers, C., 1976. Minimum entropy exchange principle-reply. *Quarterly*
970 *Journal of Royal Meteorological Society* **102**, 455–457.
- 971 Sasamori, T., 1968. The radiative cooling calculation for application to gen-
972 eral circulation experiments. *J. Appl. Meteorol.* **7**, 721–729.
- 973 Schulman, L. L., 1977. A theoretical study of the efficiency of the general
974 circulation, *J. Atmos. Sci.*, **34**, 559580.
- 975 Seager, S. and Deming, D., 2010. Exoplanet atmospheres. *Annual Review of*
976 *Astronomy and Astrophysics.* **48**, 631–672.
- 977 Sellers, W. D. 1969. A global climatic model based on the energy balance of
978 the Earth-Atmosphere system. *J. Appl. Meteor.* **8**, 392-400.
- 979 Showman, A., Cho, J.-K., Menou, K., 2010. Atmospheric Circulation of Ex-
980 oplanets. Invited review for the book "Exoplanets". S. Seager Eds., Univ.
981 Arizona Press, pp 471-516.
- 982 Showman, A. P., Fortney, J. J., Lian, Y., Marley, M. S., Freedman, R. S.,
983 Knutson, H. A., Charbonneau, D., 2009. Atmospheric circulation of hot
984 jupiters: Coupled radiative-dynamical general circulation model simula-
985 tions of HD 189733b and HD 209458b. *The Astrophysical Journal* **699**,
986 564–584.

- 987 Slingo, A., Slingo, J., 1991. Response of the national center for atmospheric
988 research community climate model to improvements in the representation
989 of clouds. *J. Geophys. Res.* **96**, 341–357.
- 990 Stephens, G., 1978. Radiation profiles in extended water clouds. II:
991 parametrization schemes. *J. Atmos. Sci.* **35**, 2123–2132.
- 992 Stephens, G., Ackermann, S., Smith, E., 1982. A shortwave parametrization
993 scheme. *J. Atmos. Sci.* **41**, 687–690.
- 994 Taylor, F., 2010. *Planetary atmospheres*. Oxford University Press.
- 995 Thrastarson H. T. and Cho J. Y-K. (2011) Relaxation Time and Dissipation
996 Interaction in Hot Planet Atmospheric Flow Simulations. *The Astrophysical Journal* **729**, 117.
- 998 Udry, S., Santos, N. C., 2007. Statistical properties of exoplanets. *Annual*
999 *Review of Astronomy and Astrophysics* **45**, 397–439
- 1000 Valencia, V., Sasselov, D. D., O’Connell, R., 2007. Radius and structure
1001 models of the first super-earth planet. *The Astrophysical Journal* **656** (1),
1002 545–551.
- 1003 Vallis, G. K., 2006. *Atmospheric and Oceanic Fluid Dynamics*. Cambridge
1004 University Press.
- 1005 Vallis, G. K., Farneti, R., 2009. Meridional energy transport in the coupled
1006 atmosphere-ocean system: scaling and numerical experiments. *Quarterly*
1007 *Journal of Royal Meteorological Society* **135**, 1643–1660.
- 1008 Wang, Y. and Read, P., 2012. Diversity of planetary atmospheric circulations
1009 and climates in a simplified general circulation model. *Proceedings IAU*
1010 *Symposium No. 293*, 2012
- 1011 Williams, D., Pollard, D., 2002. Earth-like worlds on eccentric orbits: ex-
1012 cursions beyond the habitable zone. *International Journal of Astrobiology*
1013 **1** (1), 61–69.
- 1014 Williams, D., Pollard, D., 2003. Extraordinary climates of Earth-like planets:
1015 three-dimensional climate simulations at extreme obliquity. *International*
1016 *Journal of Astrobiology* **2** (1), 1–19.

- 1017 Williams, G., P., 1988a. The dynamical range of global circulations - I. Cli-
1018 mate Dynamics **2**, 205–260.
- 1019 Williams, G. P., 1988b. The dynamical range of global circulations - II. Cli-
1020 mate Dynamics **3**, 45–84.
- 1021 Williams, G., P., 1978. Planetary circulation. I: Barotropic representation of
1022 jovian and terrestrial turbulence. *J. Atmos. Sci.* **35**, 1399–1426.
- 1023 Woollings, T., Thuburn, J., 2006. Entropy sources in a dynamical core atmo-
1024 sphere model. *Quarterly Journal of the Royal Meteorological Society* **132**,
1025 43–59.
- 1026 Wordsworth, R., Forget, F., Selsis, F., Millour, E., Charnay, B., Madeleine,
1027 J.-B., 2011. Gliese 581d is the First Discovered Terrestrial-mass Exoplanet
1028 in the Habitable Zone. *The Astrophysical Journal Letters* **733**, Issue 2,
1029 doi: 10.1088/2041–8205/733/2/L48.
- 1030 Wordsworth, R., Read, P., Yamazaki, Y., 2008. Turbulence, waves and jets in
1031 a differential heated rotating annulus experiment. *Phys. Fluids* **20**, 126602,
1032 doi:10.1063/1.2990042.

Table 1: Parameters and symbols list

parameter/symbol	explanation	value
Ω_E	Earth's rotation rate	$7.29 \cdot 10^{-5} \text{ rad}^{-1}$
c_d	specific heat of dry air	$1004 \text{ J kg}^{-1} \text{ K}^{-1}$
c_{pw}	specific heat of mixed layer model	$4180 \text{ J kg}^{-1} \text{ K}^{-1}$
g	gravitational acceleration	9.81 m s^{-2}
ρ_w	ocean water density	1030 kg m^3
h_{ml}	mixed layer depth	5 m
C_{slab}	slab-ocean areal heat capacity	$10^{-7} \text{ J K}^{-1} \text{ m}^{-2}$
α_s	surface albedo	0.2
S_0	solar constant	1365 W m^{-2}
a	planet's radius	6300 km
\mathcal{R}_o	thermal Rossby number	
\mathcal{F}_f	"frictional" Taylor number	
ASR	absorbed stellar radiation at TOA	
OLR	outgoing long wave radiation at TOA	
F_T	surface sensible heat flux	
F_{SW}^{toa}		
F_{SW}^{surf}		
F_{LW}^-		
γ_h	heat transfer coefficient	
γ_D	drag coefficient	
MHT	meridional heat transport index	
L_R	Rossby deformation radius	
N	buoyancy frequency	
α	irreversibility parameter	

1033 **Figures' captions**

- 1034 • Figure 1
1035 1(a) Schematic diagram of the $(\mathcal{F}_f, \mathcal{R}o)$ parametric space spanned in
1036 this study. Overplotted are the values of Ω^* (dashed-dotted) and τ (dot-
1037 ted). We have schematically sketched the boundaries between different
1038 circulation regimes found for dry PlaSim on the base of the circulations
1039 (AS, axisymmetric; BC, baroclinic; BT, barotropic; ZN, zonostrophic;
1040 SR, super-rotation). Circles, pentagons and triangles represent the
1041 simulations performed with $\Omega^* = 0.1, 1, 8$ respectively (see Fig.3 and
1042 2). 1(b) The same regime diagram is summarizing schematically the
1043 properties of kinetic energy dissipation (continuous line, high and low
1044 D), meridional energy transport (dotted-dashed line, high MHT), ther-
1045 mal material entropy production (dotted line, high and low \dot{S}_{sense}),
1046 efficiency (dashed line, high and low η).

- 1047 • Figure 2
1048 Zonal winds and temperature for $\Omega^* = 1/10$ ($\tau = 2700s$ (a), 1 day (b),
1049 500 days (c)), $\Omega^* = 1$ ($\tau = 2700s$ (d), 1 days (e), 500 days (f)), $\Omega^* = 8$
1050 ($\tau = 2700s$ (g), 1 days (h), 500 days (i)).

- 1051 • Figure 3
1052 As in Fig.3 but for the meridional mass streamfunction (units 10^9
1053 Kgs^{-1}).

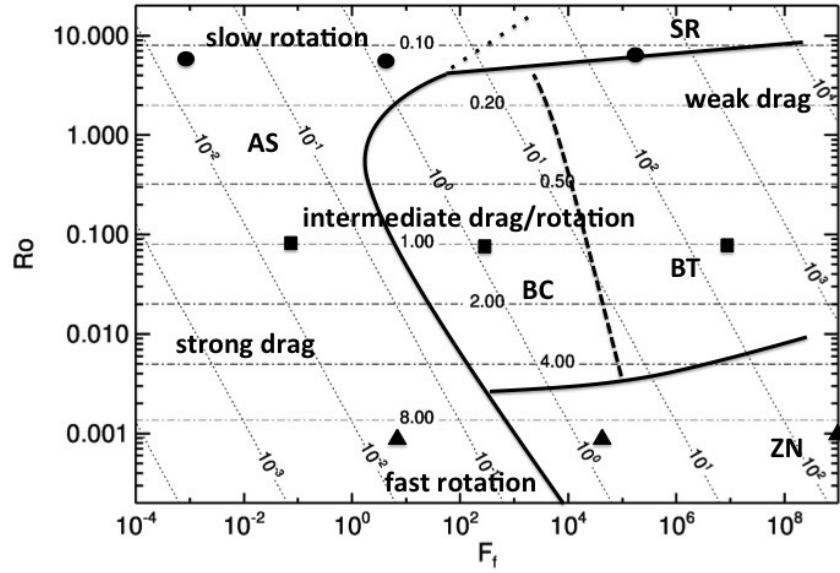
- 1054 • Figure 4
1055 Total kinetic energy dissipation; overplotted (as in all the following
1056 plots) are the values of $\log_{10} \mathcal{R}o$ (dashed) and $\log_{10} \mathcal{F}_f$ (dotted).

- 1057 • Figure 5
1058 Contribution to the total kinetic energy dissipation due to parametriza-
1059 tions representing boundary layer stresses and gravity wave drag, D_{phys} .

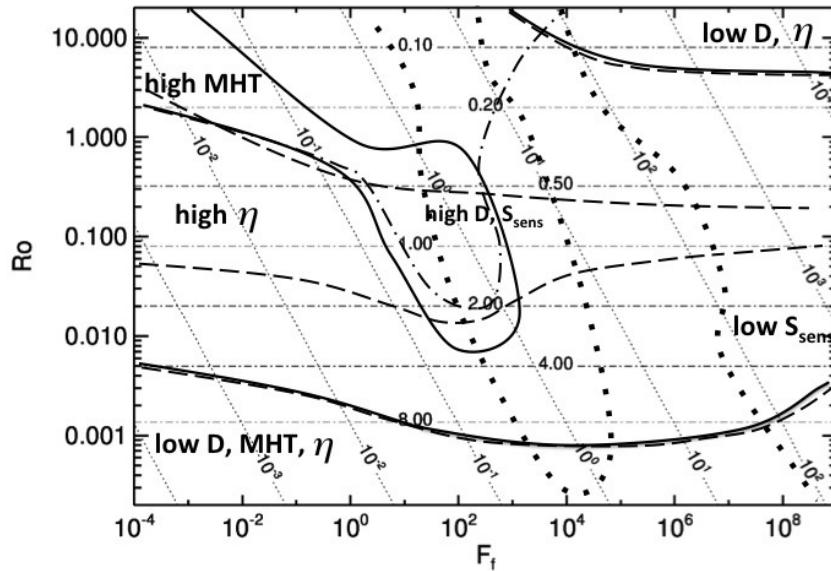
- 1060 • Figure 6
1061 Atmospheric meridional energy transport index MHT .

- 1062 • Figure 7
1063 Carnot efficiency η .

- 1064 • Figure 8
1065 Entropy production associated with surface sensible heat flux. Units
1066 in $10^{-3} \text{ W m}^{-2} \text{ K}^{-1}$.
- 1067 • Figure 9
1068 Material entropy production associated with dissipation of kinetic en-
1069 ergy. Units in $10^{-3} \text{ W m}^{-2} \text{ K}^{-1}$.
- 1070 • Figure 10
1071 Total material entropy production. Units in $10^{-3} \text{ W m}^{-2} \text{ K}^{-1}$.
- 1072 • Figure 11
1073 Irreversibility parameter α .
- 1074 • Figure 12
1075 \dot{S}_{mat} (12(a)) and $\dot{S}_{kedi ss}$ (12(b)) for the control runs BLS (continuous
1076 line), for $\tau_{max}(\Omega^*)$ maximizing \dot{S}_{mat} (dashed) and for $\tau = 0.1 \tau_{max}$ (dot-
1077 ted) and $\tau = 10 \tau_{max}$ (dotted-dashed) days. 12(c)-12(d) Same as in Fig.
1078 12(a) and 12(b) but for $\tilde{\tau}_{max}$ maximising $\dot{S}_{kedi ss}$.
- 1079 • Figure 13
1080 Zonal winds and temperature for $\Omega^* = 1/10$ (a), $\Omega^* = 1$ (b) and $\Omega^* = 8$
1081 for the BLS simulations.
- 1082 • Figure 14
1083 Meridional streamfunction for $\Omega^* = 1/10$ (a), $\Omega^* = 1$ (b) and $\Omega^* = 8$
1084 for the BLS simulations.

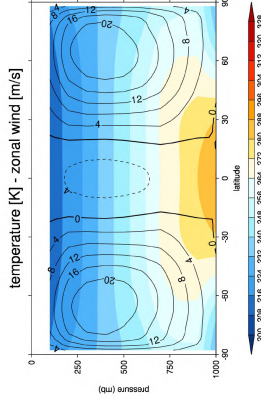


(a)

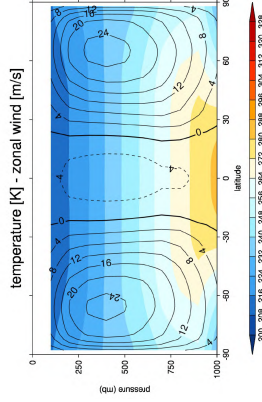


(b)

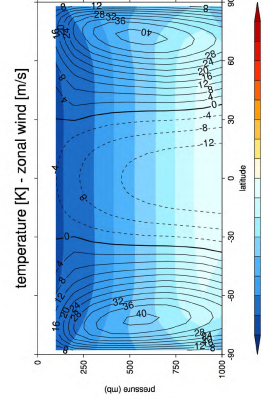
Figure 1:



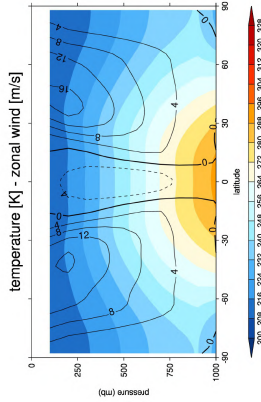
(a) $\mathcal{F}_f = 1.5 \times 10^{-3}$, $\mathcal{R}o = 8$



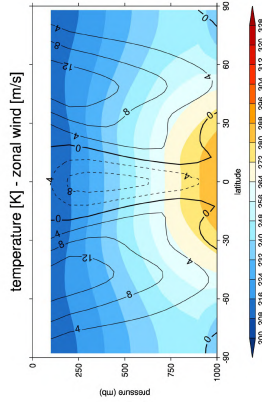
(b) $\mathcal{F}_f = 1$, $\mathcal{R}o = 8$



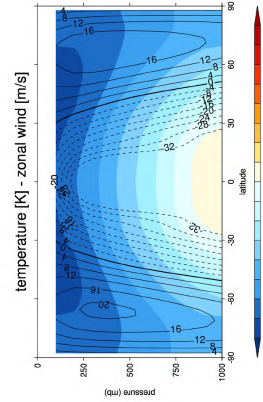
(c) $\mathcal{F}_f = 4 \times 10^5$, $\mathcal{R}o = 8$



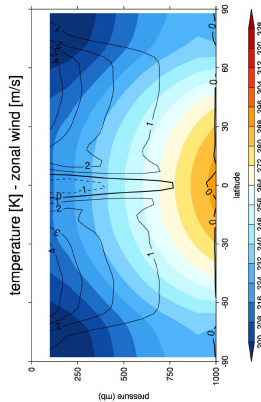
(d) $\mathcal{F}_f = 10^{-1}$, $\mathcal{R}o = 0.08$



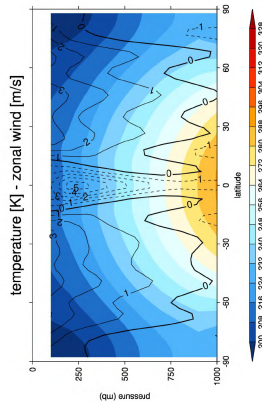
(e) $\mathcal{F}_f = 10^2$, $\mathcal{R}o = 0.08$



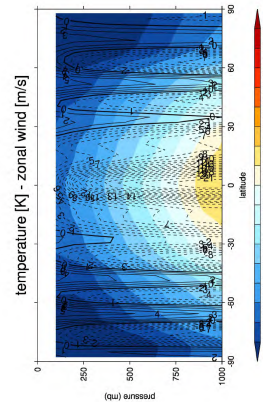
(f) $\mathcal{F}_f = 4 \times 10^5$, $\mathcal{R}o = 0.08$



(g) $\mathcal{F}_f = 10$, $\mathcal{R}o = 10^{-3}$

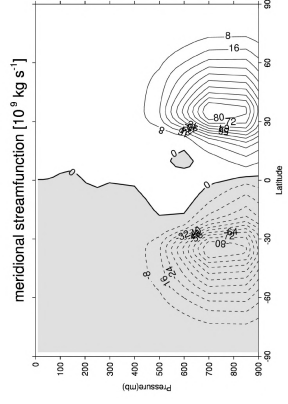


(h) $\mathcal{F}_f = 10^4$, $\mathcal{R}o = 10^{-3}$

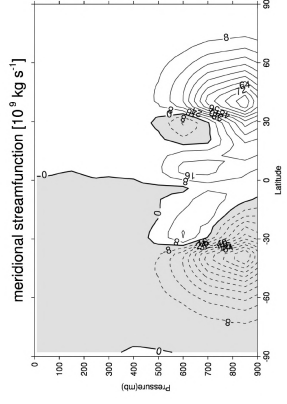


(i) $\mathcal{F}_f = 10^9$, $\mathcal{R}o = 10^{-3}$

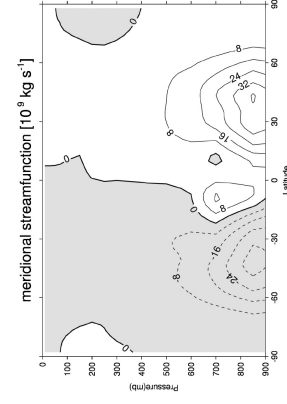
Figure 2:



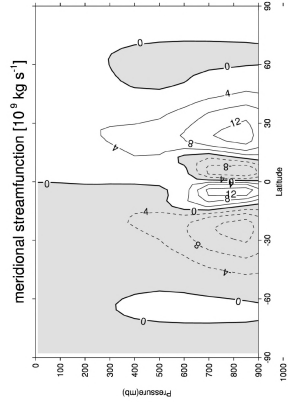
(a) $\mathcal{F}_f = 1.5 \times 10^{-3}$, $\mathcal{R}o = 8$



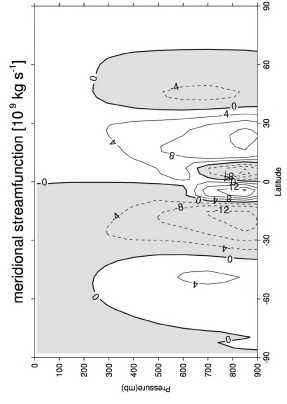
(b) $\mathcal{F}_f = 1$, $\mathcal{R}o = 8$



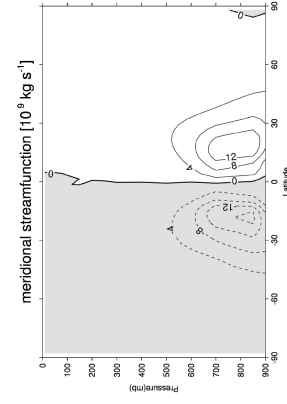
(c) $\mathcal{F}_f = 4 \times 10^5$, $\mathcal{R}o = 8$



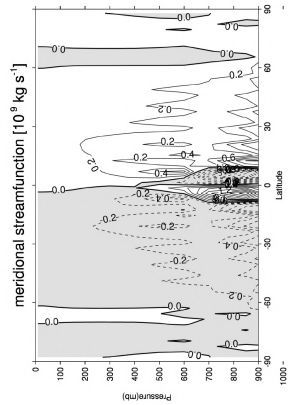
(d) $\mathcal{F}_f = 10^{-1}$, $\mathcal{R}o = 0.08$



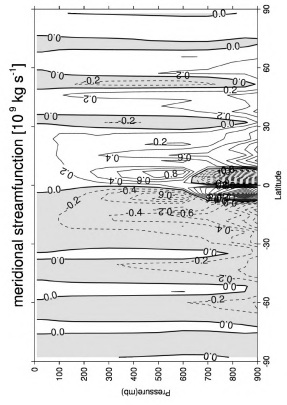
(e) $\mathcal{F}_f = 10^2$, $\mathcal{R}o = 0.08$



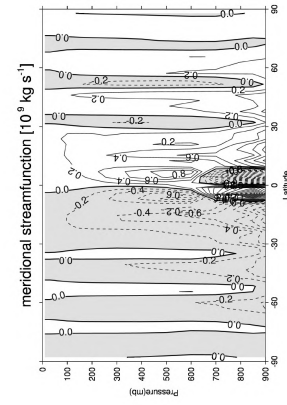
(f) $\mathcal{F}_f = 4 \times 10^5$, $\mathcal{R}o = 0.08$



(g) $\mathcal{F}_f = 10$, $\mathcal{R}o = 10^{-3}$



(h) $\mathcal{F}_f = \frac{10^4}{39}$, $\mathcal{R}o = 10^{-3}$



(i) $\mathcal{F}_f = 10^9$, $\mathcal{R}o = 10^{-3}$

Figure 3:

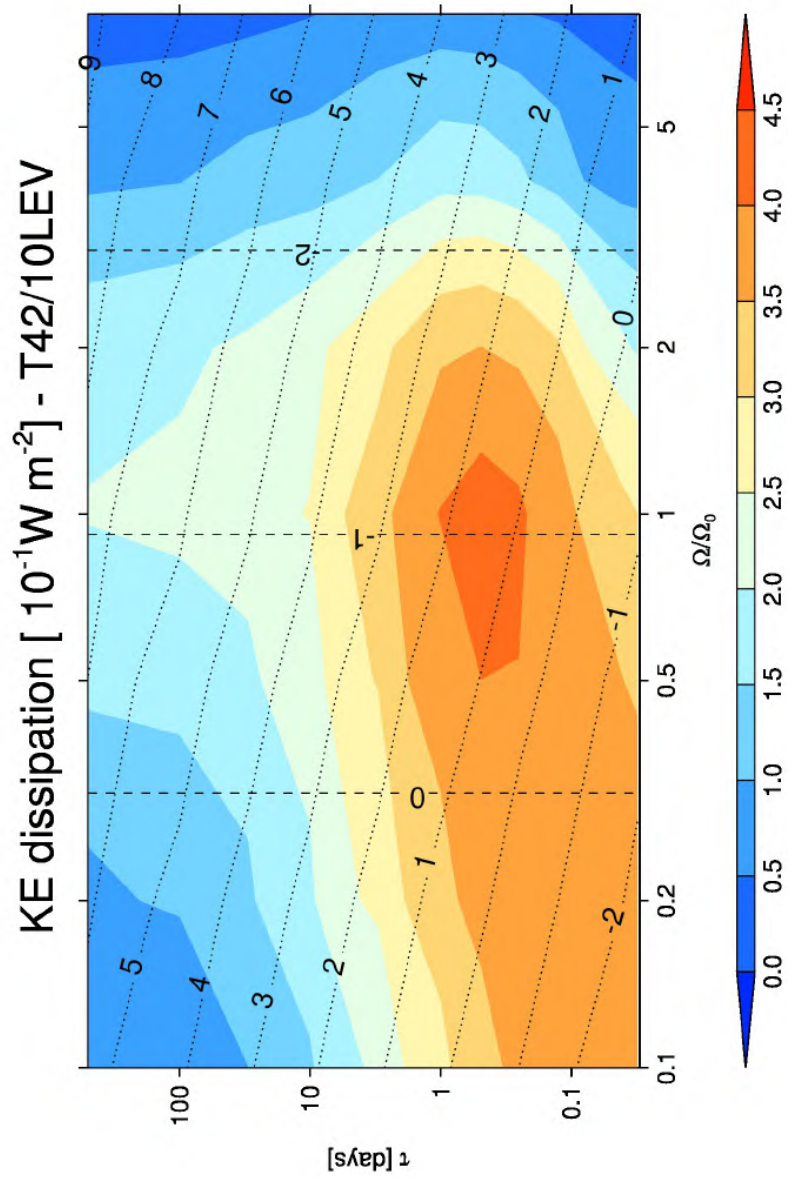


Figure 4:

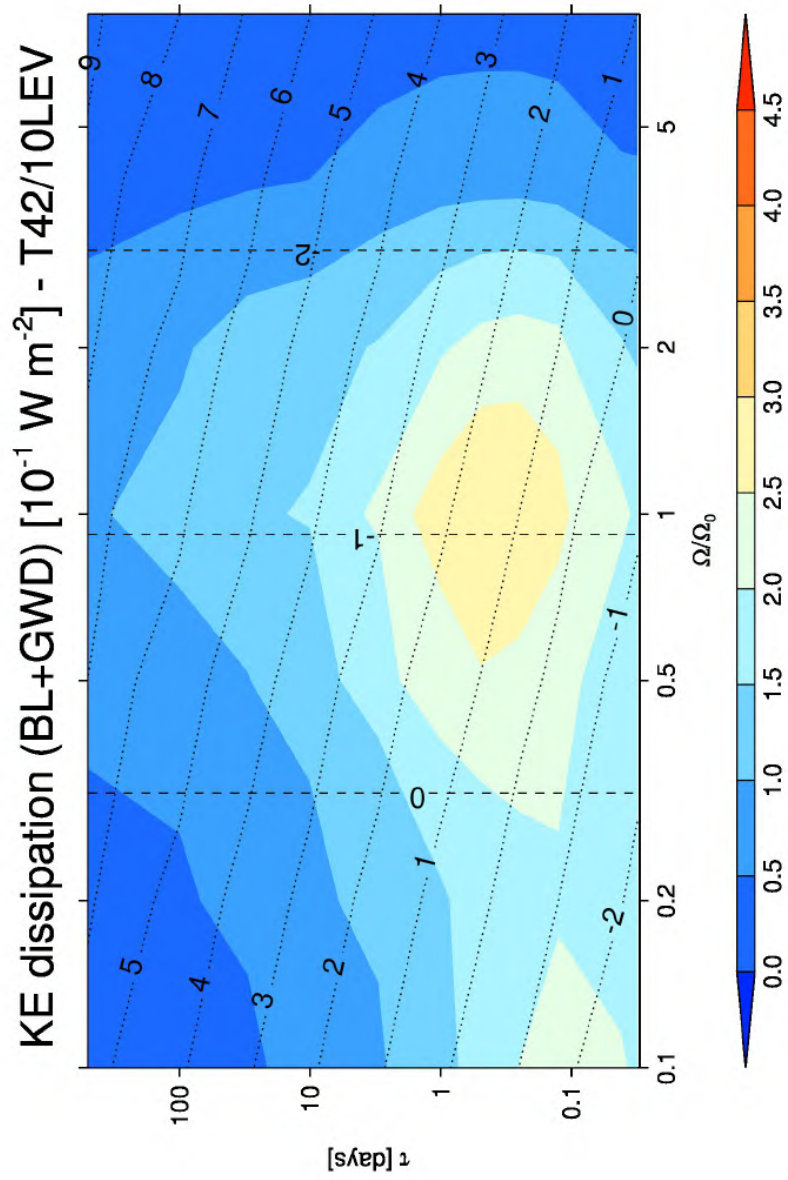


Figure 5:

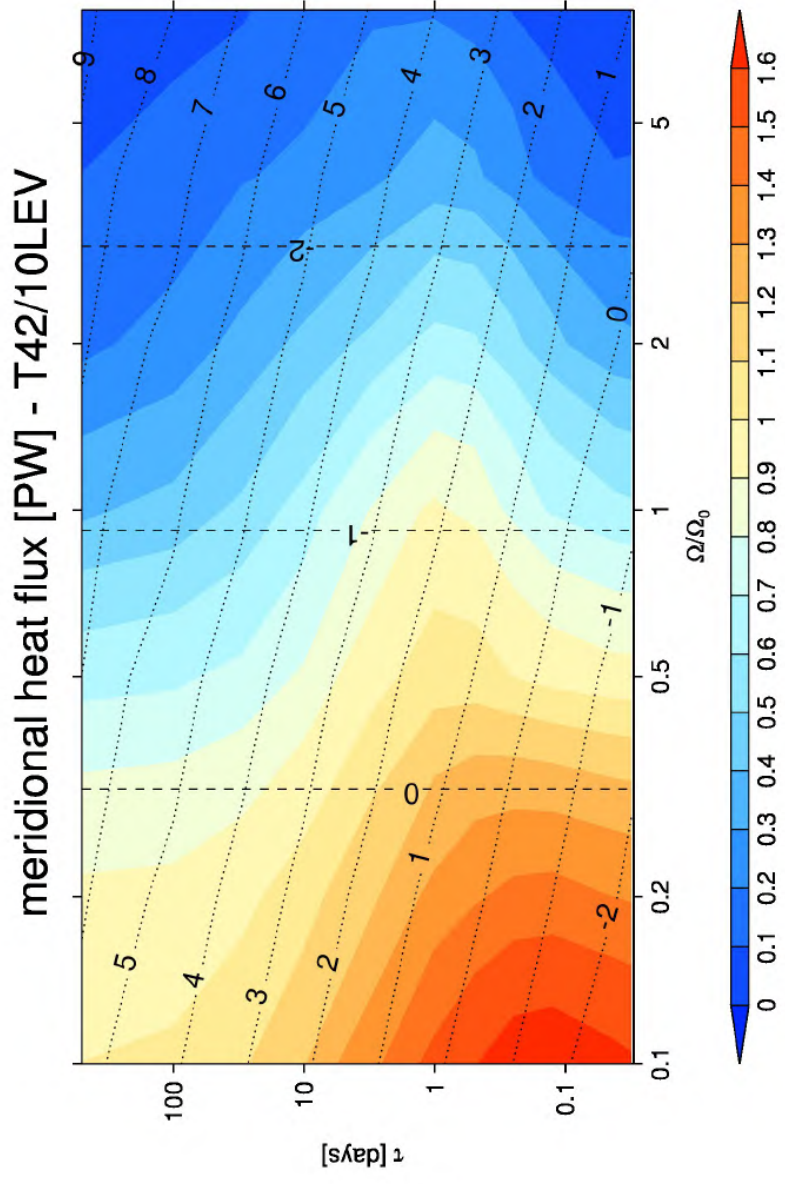


Figure 6:

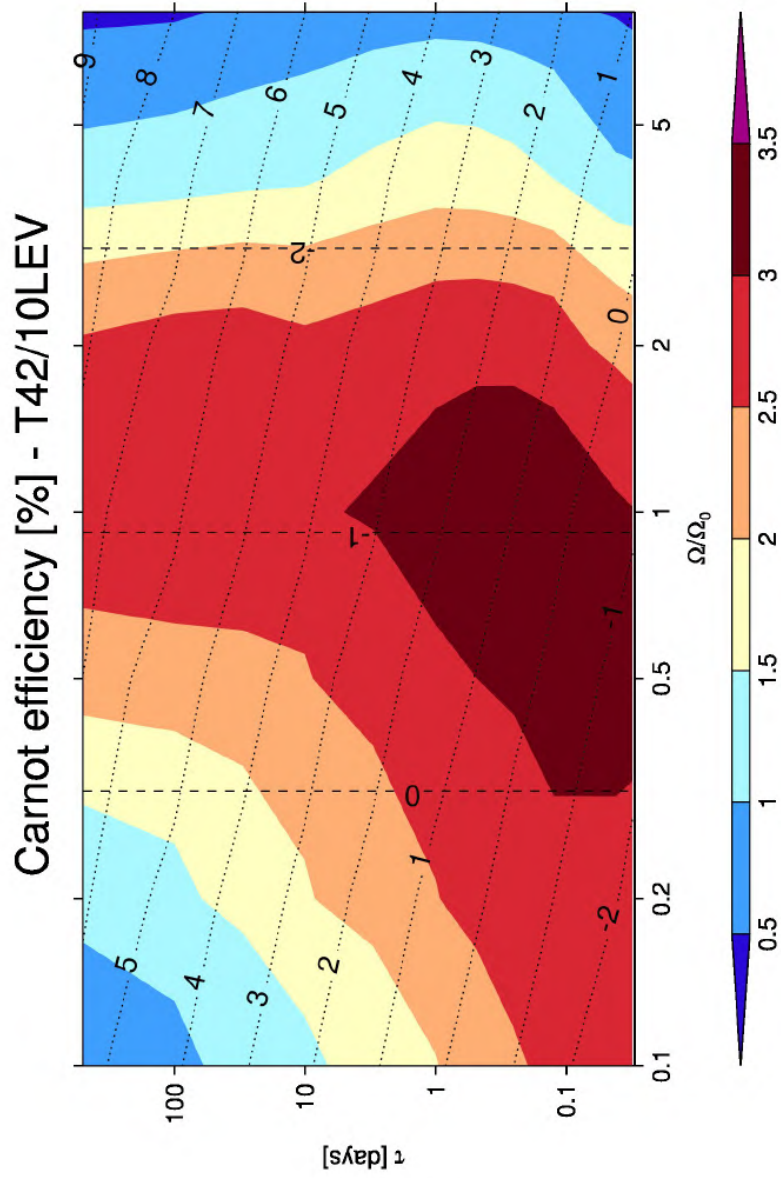


Figure 7:

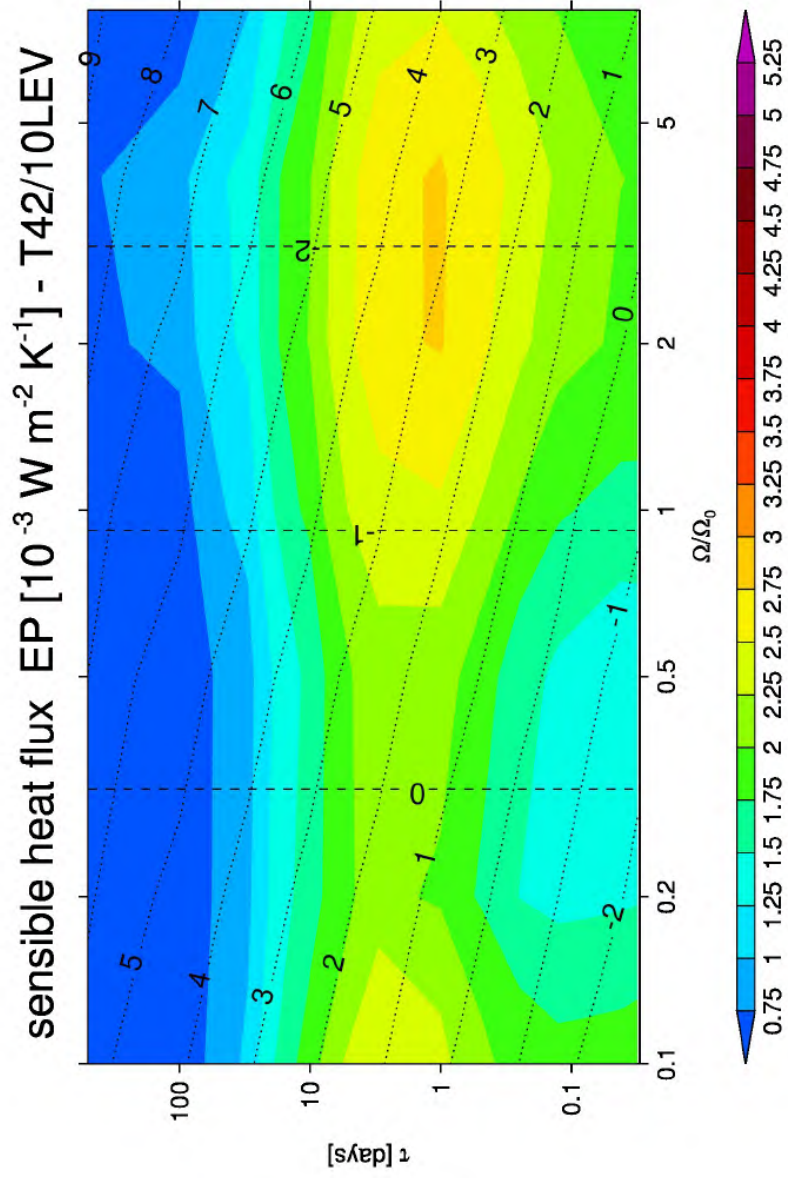


Figure 8:

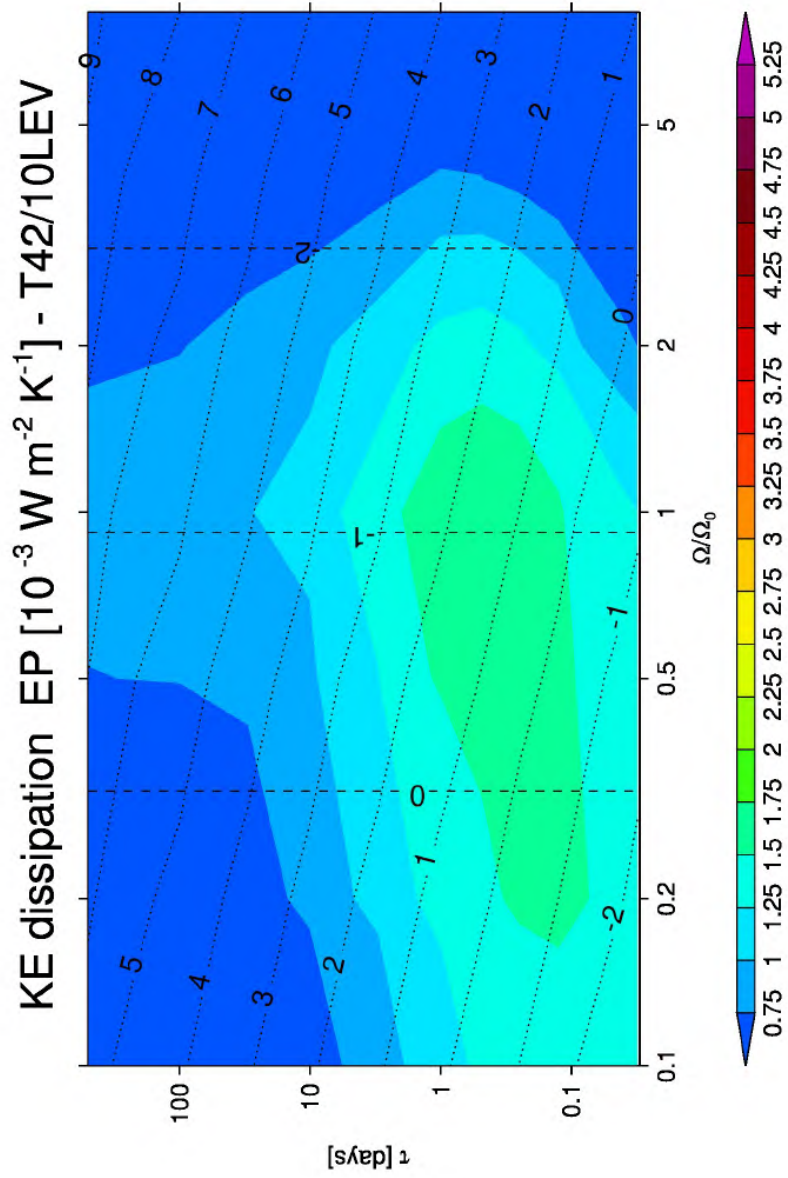


Figure 9:

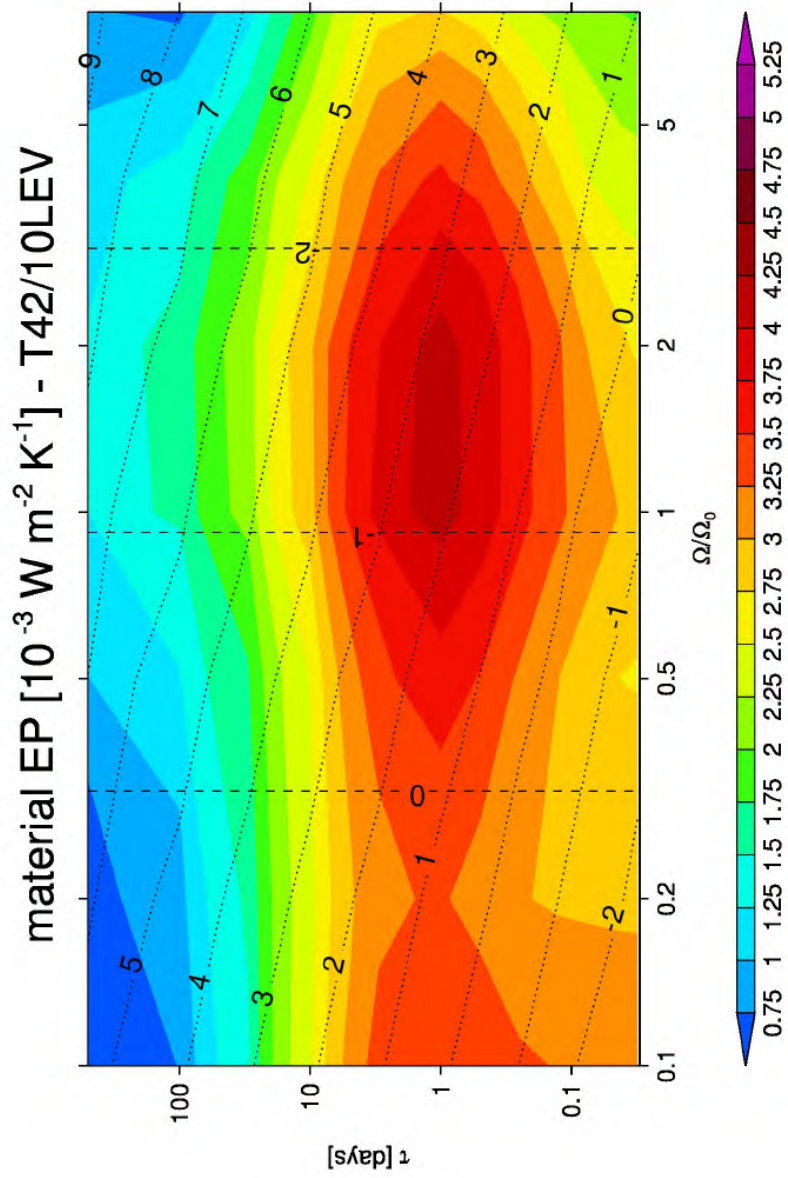


Figure 10:

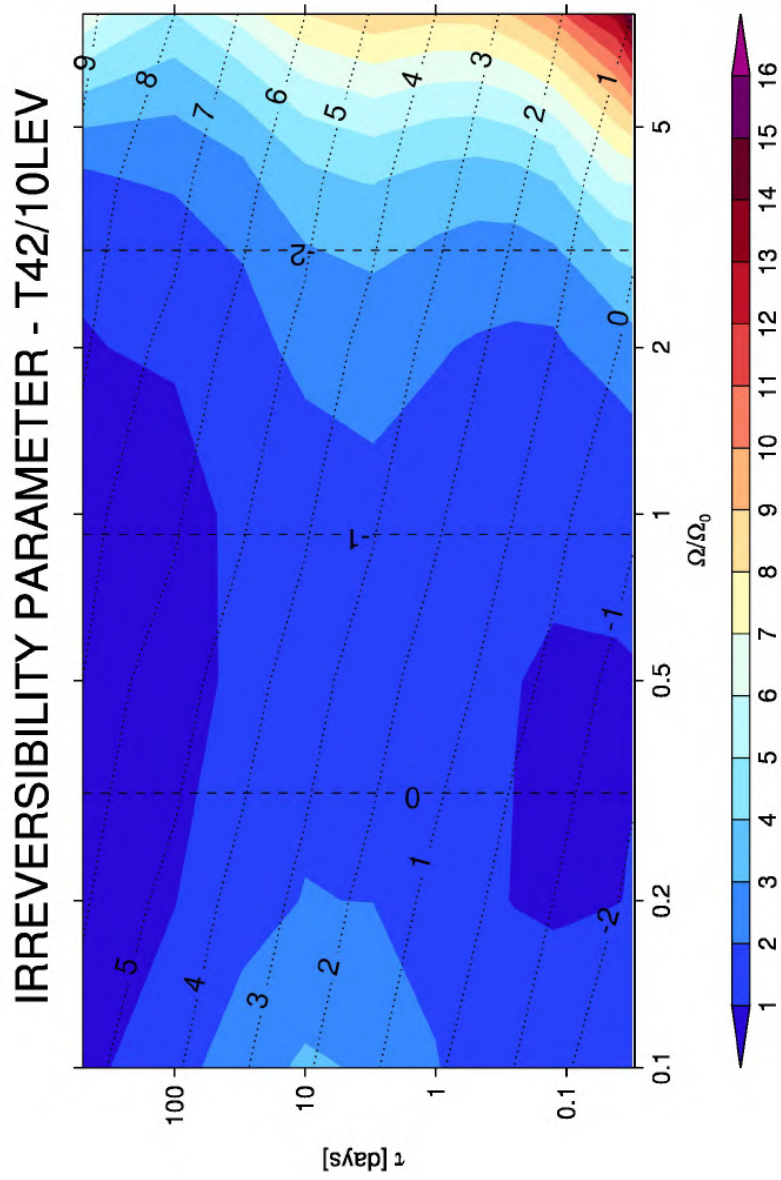
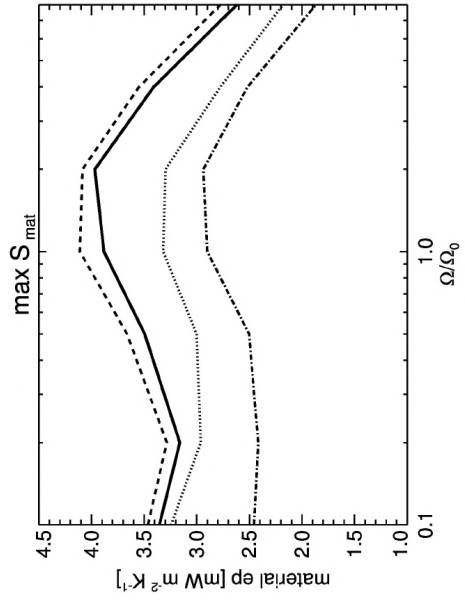
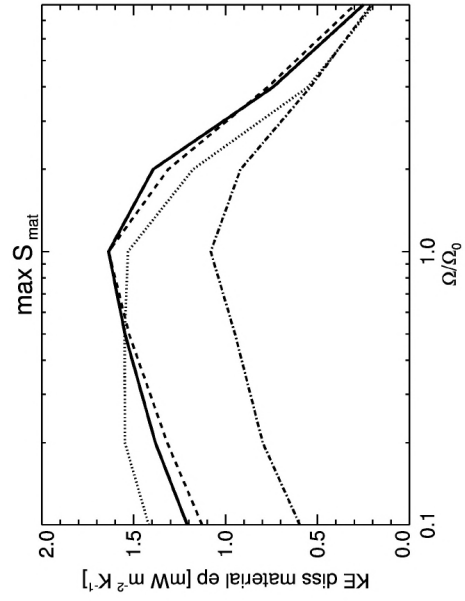


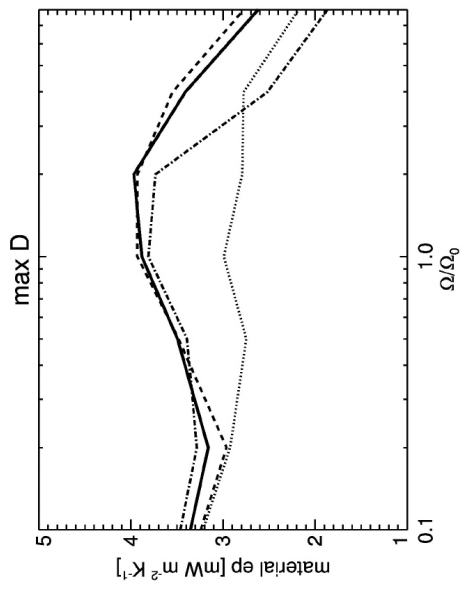
Figure 11:



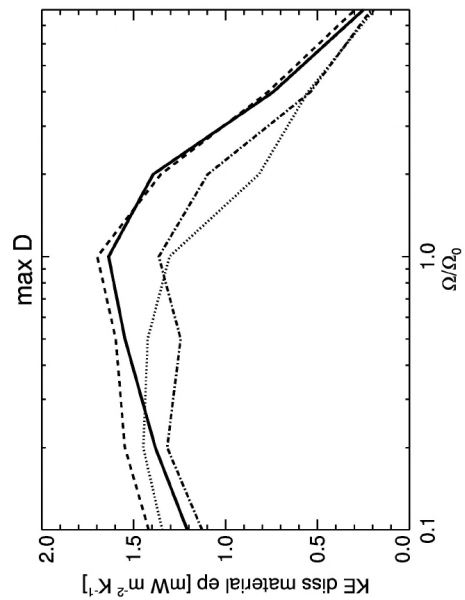
(a)



(b)



(c)



(d)

Figure 12:
48

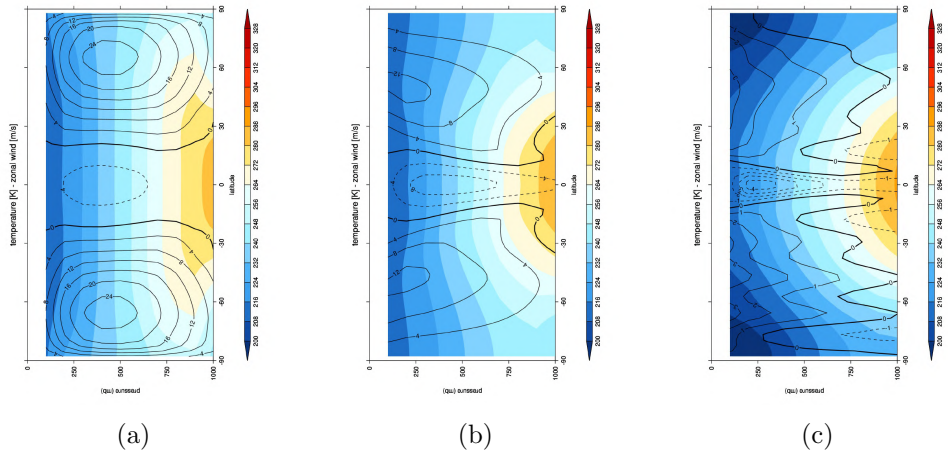


Figure 13:

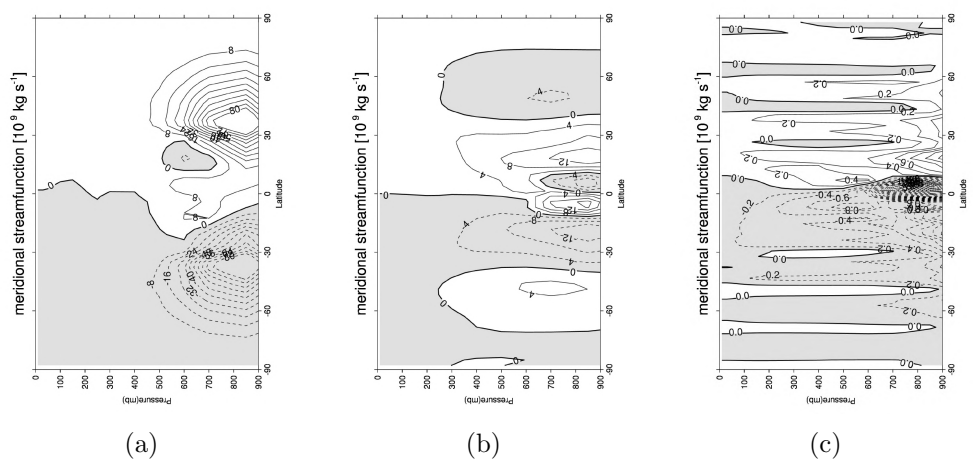


Figure 14: